Supporting information

Spatiotemporal imaging of small GTPases activity in live cells

Stephanie Voss[1,2], Dennis M. Krüger[1], Oliver Koch[3], Yao-Wen Wu*[,1,2]

[1]Chemical Genomics Centre of the Max Planck Society, Otto-Hahn-Str. 15, 44227 Dortmund, Germany;

[2]Max-Planck-Institute of Molecular Physiology, Otto-Hahn-Str. 11, 44227 Dortmund, Germany;

[3]TU Dortmund University, Faculty of Chemistry and Chemical Biology, Otto-Hahn-Str. 6, 44227 Dortmund, Germany.

*To whom correspondence should be addressed: Fax: (+49) 231 9742 6479; E-mail: yaowen.wu@mpi-dortmund.mpg.de

Methods

Protein expression and purification. All small GTPase constructs were expressed in *Escherichia coli* BL21(DE3) overnight at 18°C. Expression was induced by addition of 0.2 mM IPTG (isopropyl-β-D-thiogalactoside) at A_{600}= 0.5-0.7. For construct extraction from cell lysate Ni^{2+}-affinity chromatography (HisTrap HP, 5ml, GE Healthcare) was used. Affinity His-(Hexahistidine) tags were removed by TEV (Tobacco Etch Virus) cleavage (His-EGFP-Rab1bΔ2) or MESNA mediated transthioesterification (EGFP-Rab1bΔ2-intein-His, EGFP/EGFPD11/mCitrine-K-RasΔ4-intein-His) respectively. The affinity-tags were extracted from the protein solution by a second round of Ni^{2+}-affinity chromatography. Finally, all proteins were further purified by gel filtration chromatography using a HiLoad 16/60 Superdex 75 column or 16/600 Superdex 200 column (GE Healthcare). For the all C-terminal thioester constructs buffers without thiol were used to prevent thioester cleavage. GEF, GAP and effector proteins were purified as described earlier (DrrA$^{340-533}$, TBC1D20$^{1-362}$, OCRL1$^{539–901}$, LidA$^{201-583}$, SOS1$^{564-1049}$ and p120GAP$^{714-1047}$)[1-4].

Protein labeling. For cysteine labeling EGFP/mCitrine-tagged protein constructs were transferred into thiol free GTPase buffer (20 mM HEPES pH 7.5, 20 mM NaCl, 1 mM $MgCl_2$, 10μM GDP) by size exclusion Sephadex G-25 columns (GE Healthcare). Tide Fluor 3 maleimide (AAT Bioquest) was added from a 10 mM stock solution in DMSO in a 1.5-2.5 molar excess to the protein. The mixture was incubated at 25°C for 30-120 min. After labeling was completed as confirmed by ESI-MS and fluorescence measurements, unreacted dye was removed by a second G-25 size exclusion with thiol containing buffer (20 mM HEPES pH 7.5, 20 mM NaCl, 1 mM $MgCl_2$, 10μM GDP, 2 mM DTE (Dithioerythritol)) for EGFP-Rab1bΔ2 constructs or thiol free GTPase buffer for C-terminally thioester tagged constructs.

Expressed protein ligation. For reconstitution of the C-terminal prenylation motif, the labeled protein-thioester constructs were transferred into freshly prepared and degassed ligation buffer (20 mM HEPES pH 7.5, 50 mM NaCl, 1 mM $MgCl_2$, 10 μM GDP) using G-25 size exclusion columns. The protein solution was concentrated to 100 μl (5-10 mg/ml) and mixed with 50 μl ligation buffer containing TCEP (tris(2-carboxyethyl)phosphine), MPAA (4-mercaptophenylacetic acid) and the peptide CC for Rab1 or CVIM for K-Ras respectively, to a final concentration of 20 mM TCEP, 50 mM MPAA and CC/CVIM 2 mM. The ligation mixture was incubated at 4°C overnight. Finally the ligation product was transferred to GTPase buffer containing 20 mM HEPES pH 7.5, 20 mM NaCl, 1 mM $MgCl_2$, 10μM GDP and 2 mM DTE, using size-exclusion concentrators (molecular-weight cutoff 30 kDa, Millipore).

Cell culture

All cell lines were cultured in 100 mm tissue culture dishes and 7-8 ml minimum essential medium (MEM) supplemented with 10 % (v/v) fetal bovine serum (FBS), 1 % (v/v) sodium pyruvate solution (100 mM), 1 % GlutaMAX and 1 % (v/v) non-essential amino acids at 37 °C and 5 % CO_2. Cells were split every two to three days at a confluency of 70-80 %. After washing with 5 ml dulbecco's phosphate-buffered saline (DPBS) cells were detached by incubation with 1 ml 0,25 % (v/v) trypsin-EDTA at 37 °C and 5 % CO_2. Complete detachment was confirmed by microscopy and the cells

suspended in 4-9 ml supplemented MEM. Finally, 1 ml of the cell suspension were mixed in 7 ml supplemented MEM in a new 100 mm tissue culture dish. Cells were tested regularly (once every month) for mycoplasma contamination.

For transfection 0.5-1 ml cell suspension was added to a mixture of 1-3 μg plasmid DNA preincubated 15-20 min in 200 μl Opti-MEM (Thermo Fisher Scientific) with 1-2 μl X-tremeGENE HP transfection reagent in a 35 mm glass bottom dishes (MatTek Corporation). After transfection the cells were incubated overnight at 37 °C and 5 % CO_2 and subsequently used for microscopy or microinjection.

The following ATCC cell lines where used in this work: HeLa, ATCC ID: CCL-2; COS-7, ATCC ID: CRL-1651; MDCK, ATCC ID: CCL-34.

Fluorescence and fluorescence polarization measurements. Spectra acquisition, time-dependent sensitized emission and fluorescence polarization measurements were performed with a FluoroMax-3 spectrofluorometer (Horiba Jobin Yvon). All measurements were performed at 25 °C in freshly degassed buffer containing 20mM HEPES pH 7.5, 20 mM NaCl, 1 mM $MgCl_2$, 2 mM DTE. Fluorescence spectra were collected by exciting at 480 nm and collecting emission at 490-700 nm. FRET was observed with excitation at 480 nm and emission collected at 580 nm (TF3) or 614 nm (TF4). Binding of effector proteins was independently monitored by fluorescence polarization with excitation at 480 nm and emission collected at 510 nm.

Quantitative nucleotide exchange

For quantitative nucleotide exchange the following protocol was used. EDTA was added in a five times molar excess with respect to the Mg^{2+} concentration in the buffer. To this mixture the desired target nucleotide was added in a 5- (for mantGDP) or 20-times (for GppNHp) molar excess with respect to the GDP concentration and incubated at room temperature for at least 2 h. Finally EDTA was removed by transferring the protein into buffer containing 20 mM HEPES pH 7.5, 50 mM NaCl, 1 mM MgCl2, 2 mM DTE and the desired nucleotide at a concentration of 1 μM for mantGDP or 10 μM for GppNHp respectively, using a NAP-5 Column.

Microinjection of sensor constructs

For microinjection the sensor constructs were concentrated to 6-10 mg/ml and microinjected into 40-70 cells using an Eppendorf Transjector 5246 and Eppendorf Micromanipulator 5171. Before imaging the microinjected cells were incubated at 37 °C for 1 h.

Confocal and fluorescence lifetime imaging microscopy

Confocal and fluorescence lifetime imaging microscopy were carried out using the laser scanning confocal microscope FlouView FV1000 (Olympus Deutschland GmbH) equipped with a time-correlated single-photon counting (TCSPC) LSM Upgrade Kit (PicoQuant). Cell images were collected

through a 60x/1.35 UPlanSApo oil immersion objective (Olympus Deutschland GmbH, Hamburg, Germany). Ni-NTA bead images were collected through a 40x/1.35 UPlanSApo air objective (Olympus Deutschland GmbH). For FLIM measurements the samples were excited with a 470 nm pulsed diode laser (LDH 470, PicoQuant, Berlin, Germany) at a repetition rate of 40 MHz. The photons were collected in a single-photon counting avalanche photodiode (PDM Series, MPD, PicoQuant) and timed using a time-correlated single-photon counting module (PicoHarp 300, PicoQuant) after being spectrally filtered using a narrow-band emission filter (HQ 525/15, Chroma). All measurements were carried out in a live-cell imaging chamber with control of humidity, temperature of 37°C and 5% CO_2. FLIM analysis was performed using global analysis[2].

Statistical analysis

Data in figure 3 and 6 are shown as mean ± s.d. with sample numbers indicated in figure legends. Box plots are presented as: - median, □ mean, upper hinge 75th percentile, lower hinge 25th percentile, whiskers: s.d., and with all data points plotted. All suitable cells in each sample were quantified and the sample size was deemed appropriate based on the s.d. being smaller than the observed effects and the appropriate control experiments displaying the same variance.

Microscopy images and fluorescence measurements are representative from at least three experiments. Statistical significance was determined by unpaired two-tailed t-tests. Fits were performed using Origin 8.6 and GraFit 5.

MD simulations

MD simulations were conducted with AMBER14 on GPU using Sander for minimization and equilibration, and PMEMD for the production runs in explicit water[7–9]. Force field parameters for GDP and GTP were taken from Meagher *et al.*[10], and for Mg^{2+} from Allnér *et al.*[11]. Protein atoms and counterions were described by the ff14SB forcefield[12,13]. All model systems were generated with LEaP. Each model system was placed in an octahedral TIP3P water box with an extension of at least 11 Å in each direction from the solute and neutralized by adding Na^+ or CL^- counterions[14]. Solvated systems were then subjected to a two-step minimization procedure in order to remove clashes between the water molecules and the solute: (1) 50 steps of steepest descent and 200 steps of conjugate gradient minimization with harmonic positional restraints of strength 25 kcal mol^{-1} A^{-2} on all solute atoms, (2) 50 steps of steepest descent and 200 steps of conjugate gradient minimization with harmonic positional restraints of strength 5 mol^{-1} A^{-2} on all solute atoms. After minimization, four steps of equilibration were run: (1) 50 ps NVT simulation to increase the thermostat target temperature from 100 K to 300 K using Berendsen's temperature and pressure control algorithms with time constants of 0.5 ps for both heat bath coupling and pressure relaxation, (2) 50 ps NPT simulation at constant isotropic pressure of 1 atm to adjust the density of the system to 1 g cm^{-3}, (3) five 50 ps NVT simulations progressively decreasing the restraints in steps of 1 kcal mol^{-1} A^{-2}, and finally (4) 50 ps NVT simulation without any restraints[15].

The equilibrations were followed by 500ns production simulations. The simulation timestep was 2fs and snapshots were saved every 20ps. During dynamics the SHAKE algorithm was used to constrain all bonds involving hydrogen atoms[16]. A 8 Å cutoff radius was used for short-range non-bonded interactions. Long-range interactions were treated by the Particle Mesh Ewald method[17,18]. The temperature was kept constant at 300K using Berendsen's weak coupling algorithm[15]. Production simulations were carried out under NVT conditions.

Root-mean-square fluctuation (RMSF) analyses of the MD trajectories were performed employing CPPTRAJ based on the Cα-atoms[19]. The first 50ns were not considered for the analysis to neglect perturbations due to substrate adaption, respectively. Backbone Root-mean-square deviations (RMSD) revealed that all systems remained stable over the residual simulation time of 450ns (data not shown).

Supplementary Figure S1 MD simulations

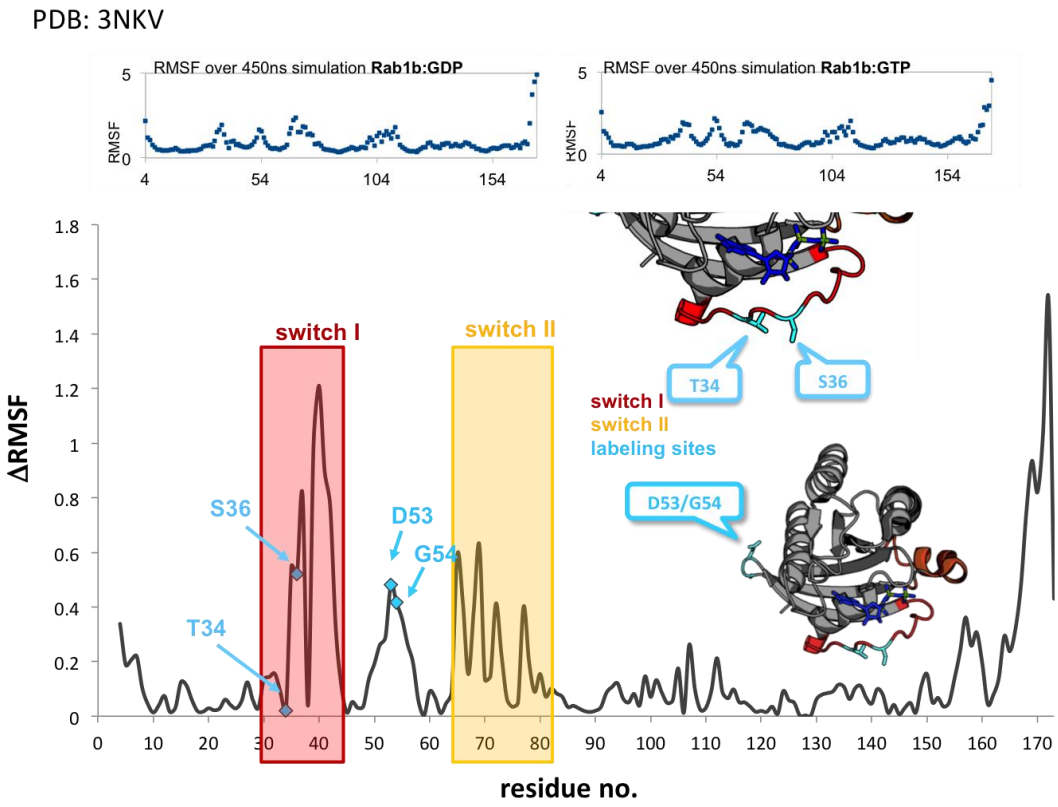

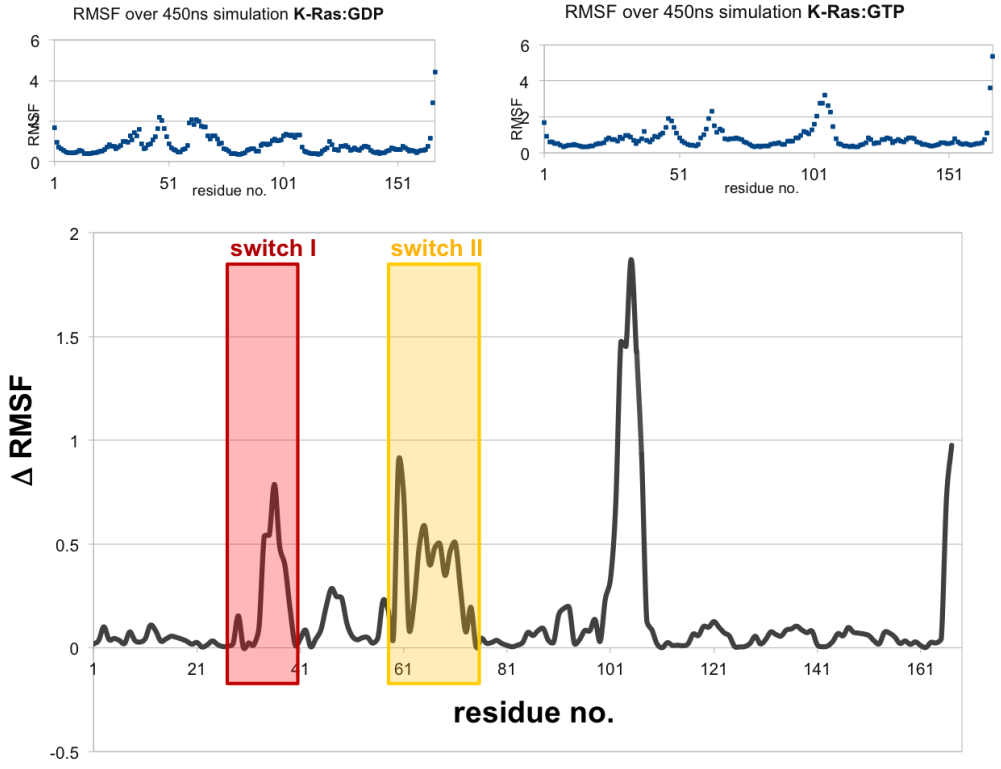

Figure S1 Molecular dynamics (MD) simulations of the root mean square fluctuation (RMSF) in GTP- and GDP-bound Rab1 and K-Ras.

MD simulations of Rab1 were based on the X-ray structure of Rab1 bound to GppNHP (PDB: 3NKV). Modified AMP at Y77 was removed and GppNHP was changed to either GDP or GTP. MD simulations of K-Ras were based on the X-ray structure of K-RasQ61H bound to GppNHP (PDB: 3GFT). The Q61H mutation was restored and GppNHP was changed to either GDP or GTP. For all structures incomplete residues were repaired using Maestro[6].

Supplementary Figure S2 Structural analysis of known Rab complexes

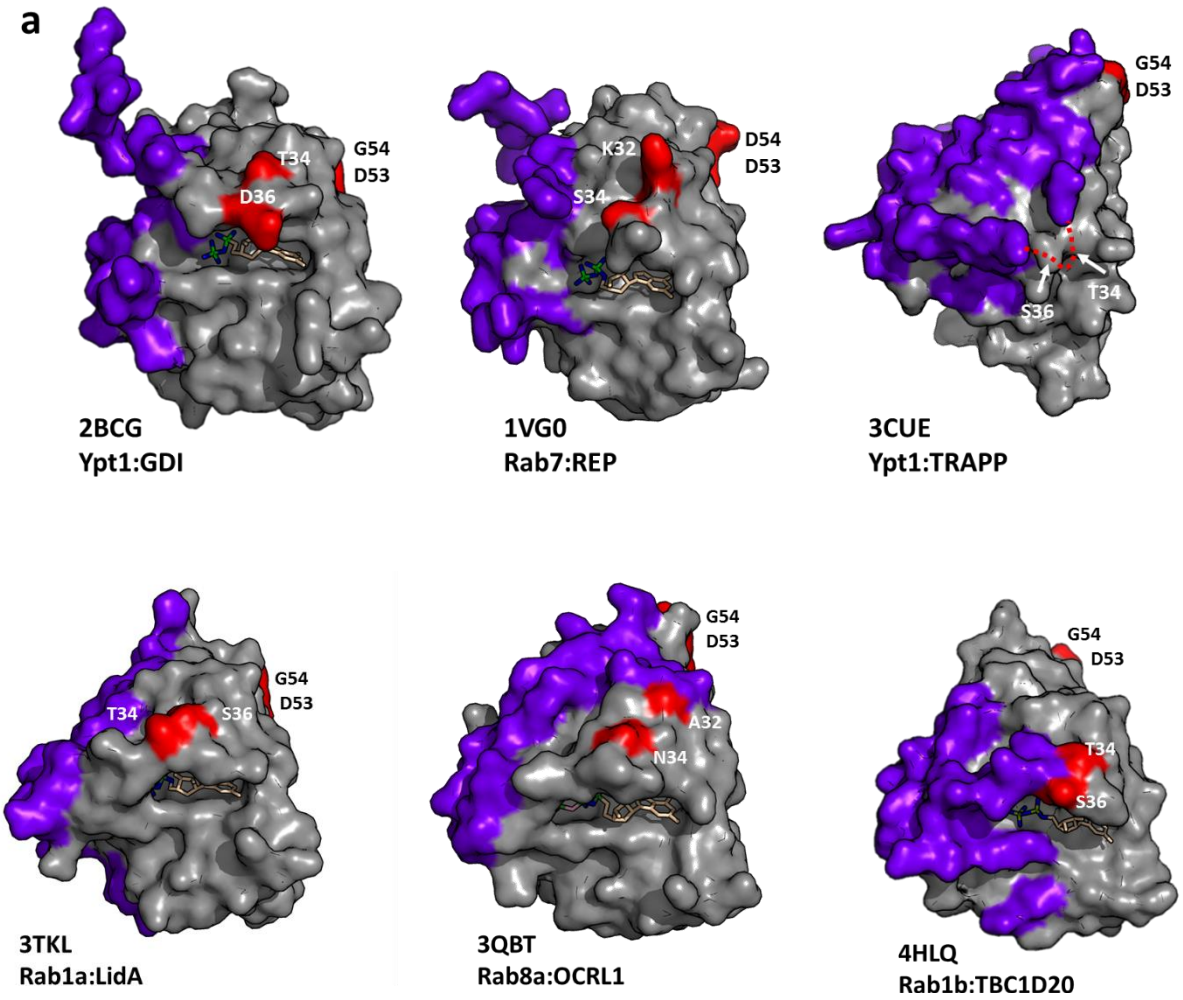

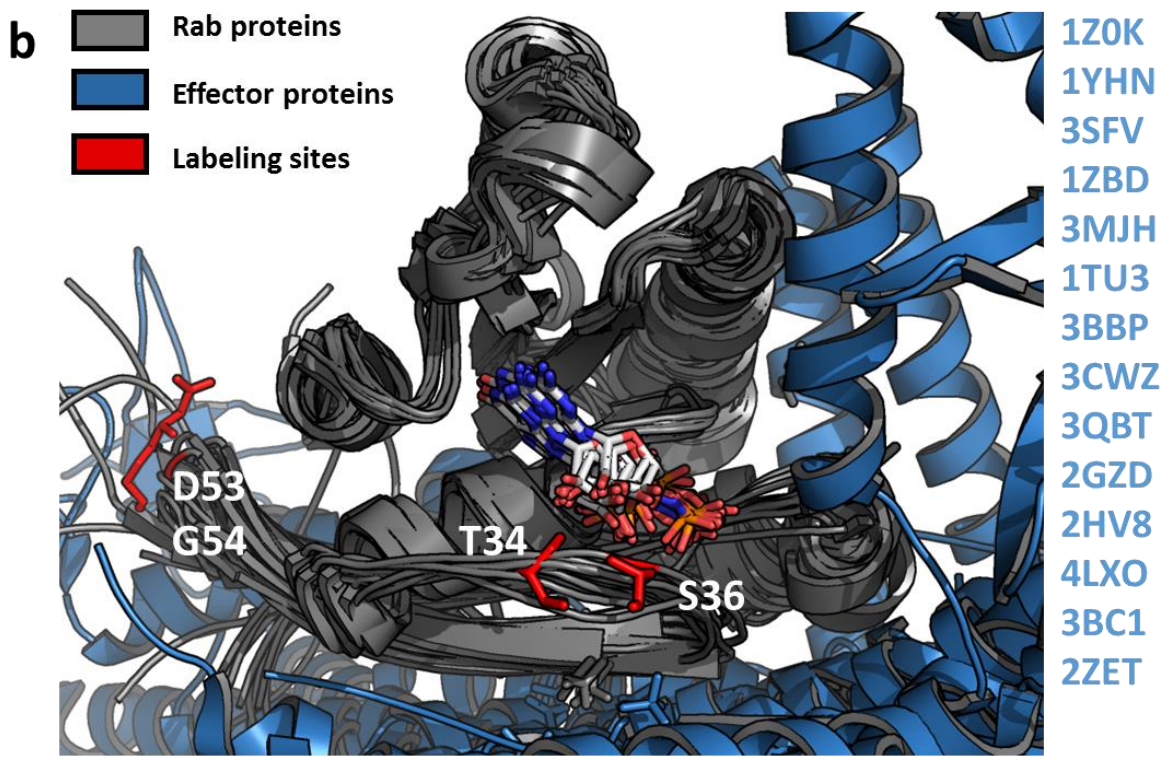

Figure S2 Structural analysis of known Rab complexes.

(a) **Surface representation of Rab proteins shows the interacting residues involved in regulators/effectors binding.** Interacting sites of Rab in complex with GEF, GAP, effectors, GDI and REP are marked in purple. The labeling sites of Rab1 COSGA sensors are highlighted in red. In the Ypt1:TRAPP complex the labeling residues (T34 and S36), are not resolved in the crystal structure, indicating structural flexibility of this region. (b) Alignment of Rab:effector structures. Rab GTPases are displayed in grey. Rab effectors are depicted in blue. GTP is shown in stick mode. The labeling sites T34, S36, D53 and G54 are marked in red.

Supplementary Figure S3 Protein labeling

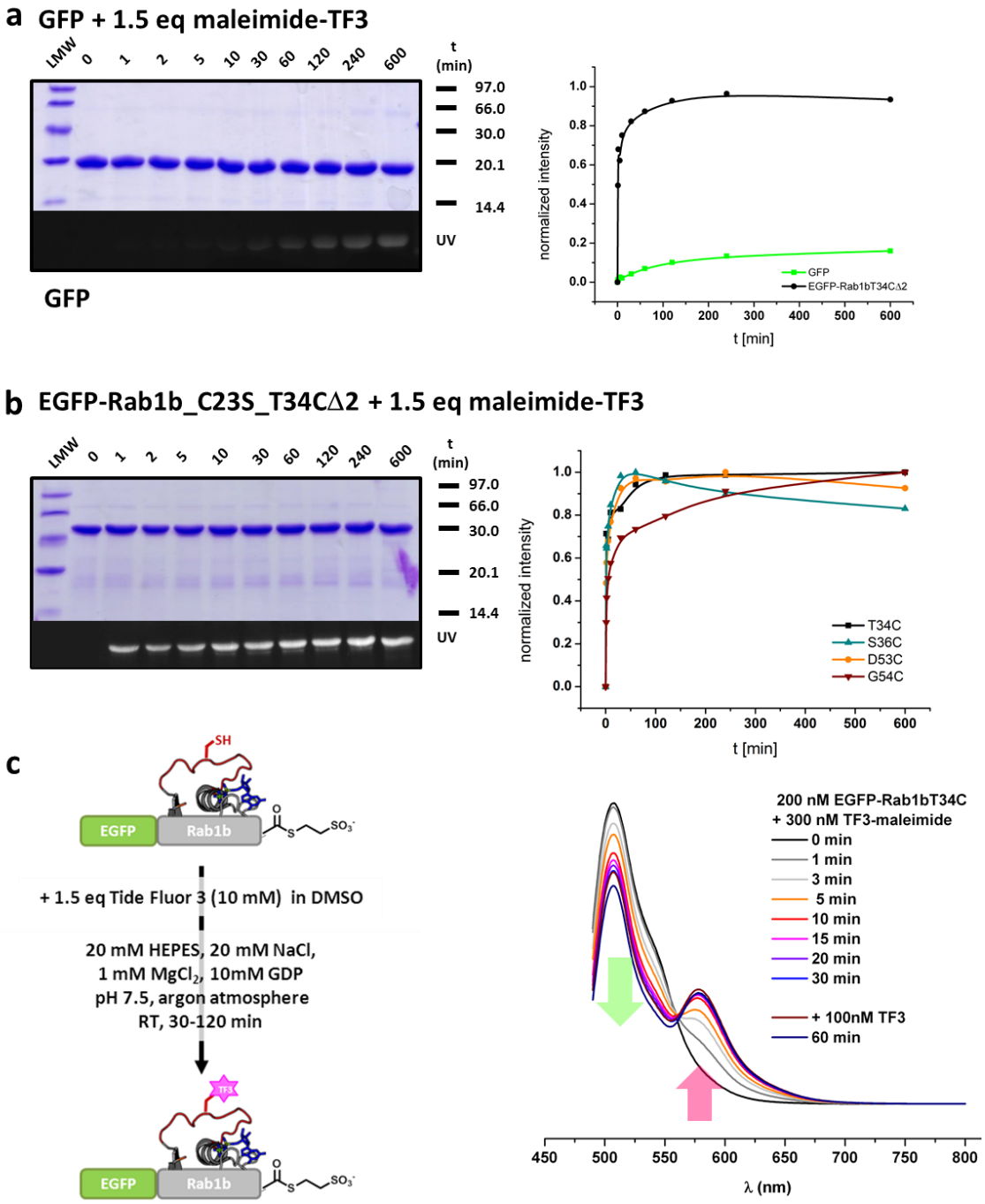

Figure S3 Site-specific protein labeling

(a) The direct labeling of GFP was tested under the same conditions as the sensor constructs and shows only negligible labeling in comparison to the **(b)** GTPase with cysteine mutants. Intrinsic cysteine residues of Rab1 were mutated (C23S) or truncated (Δ2). **(c)** The labeling process can also be monitored by FRET (decrease of the donor emission and increase of the acceptor emission) with excitation at 480 nm.

Supplementary Figure S4 LC-ESI-MS

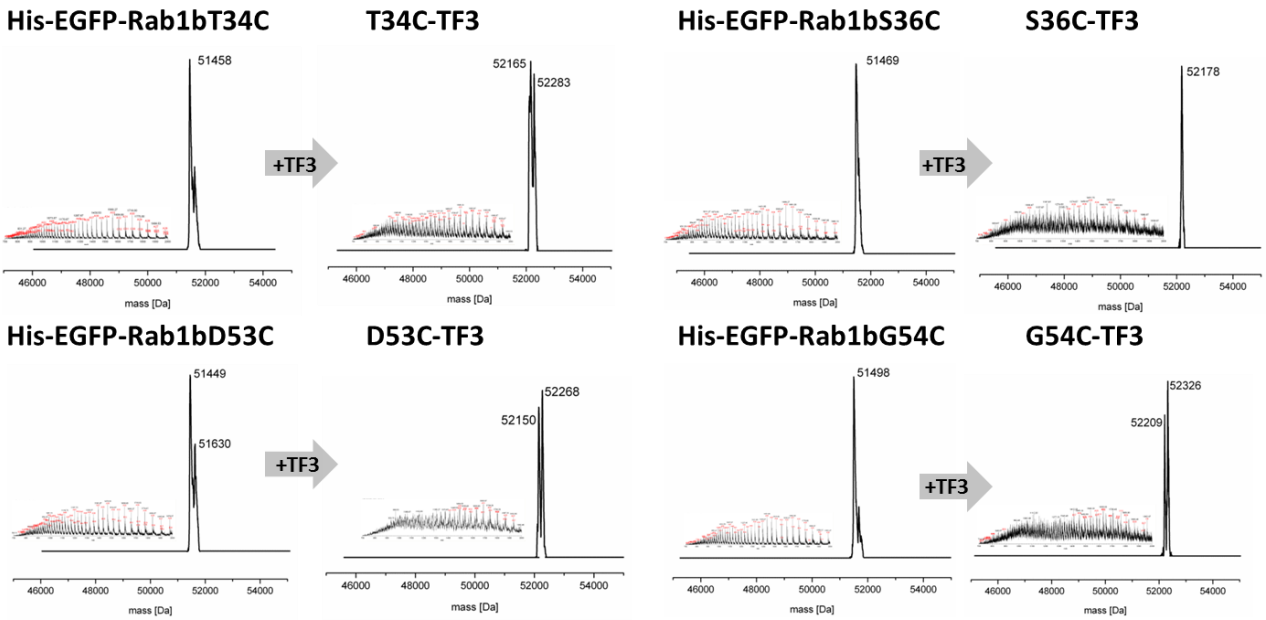

Tide Fluor™ 3 maleimide [TF3 maleimide] M = 651.71 g/mol

protein	calculated	observed
His-EGFP-Rab1bT34C-COOH	51470	51458 (Δ= -12)
His-EGFP-Rab1bS36C-COOH	51484	51469 (Δ= -15)
His-EGFP-Rab1bD53C-COOH	51456	51449 (Δ= -7)
His-EGFP-Rab1bG54C-COOH	51514	51498 (Δ= -16)

protein-TF3	calculated	observed
His-EGFP-Rab1bT34C-COOH	52181	52165 (Δ=-16)
His-EGFP-Rab1bS36C-COOH	52195	52178 (Δ=-17)
His-EGFP-Rab1bD53C-COOH	52167	52152 (Δ=-15)
His-EGFP-Rab1bG54C-COOH	52225	52209 (Δ=-16)

EGFP-Rab1bT34C-MESNA

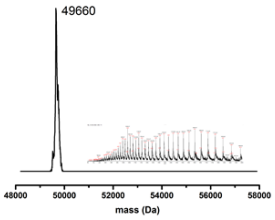

EGFP-Rab1bQ67L_T34C-MESNA

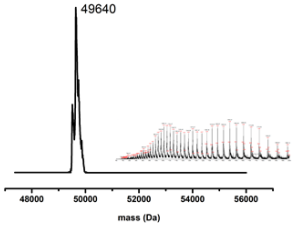

EGFP-Rab1bS36C-MESNA

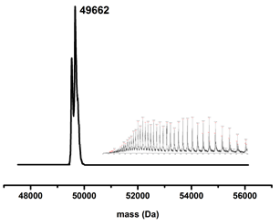

EGFP-Rab1bD53C-MESNA

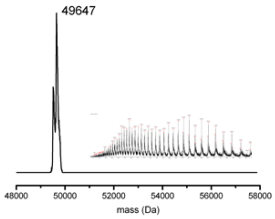

EGFP-Rab1bG54C-MESNA

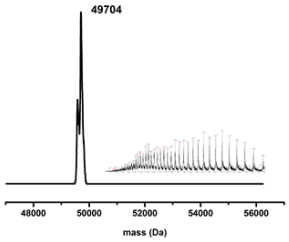

protein	calculated	observed
EGFP-Rab1bT34C-MESNA	49670	49660 (Δ=-10)
EGFP-Rab1bQ67LT34C-MESNA	49665	48640 (Δ=-15)
EGFP-Rab1bS36C-MESNA	49668	49662 (Δ=-6)
EGFP-Rab1bD53C-MESNA	49640	49647 (Δ=-7)

protein	calculated	observed
EGFP-Rab1bG54C-MESNA	49698	49704 (Δ=-6)

Tide Fluor™ 3 maleimide [TF3 maleimide] M = 651.71 g/mol
***does not include a C23S mutation**

EGFP-Rab1bT34C-TF3-CC

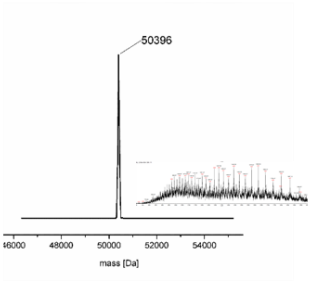

EGFP-Rab1bQ67L_T34C-TF3-CC

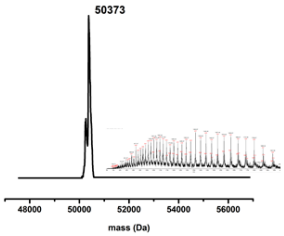

EGFP-Rab1bS36C-TF3-CC

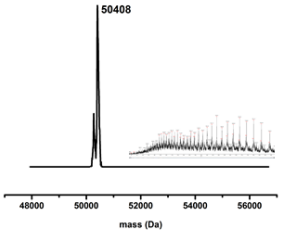

EGFP-Rab1bD53C-TF3-CC

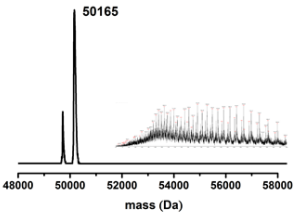

EGFP-Rab1bT34C-CC

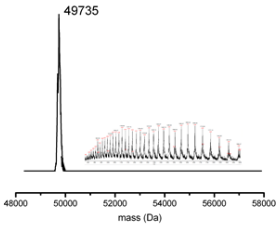

EGFP-Rab1bS36C-CC

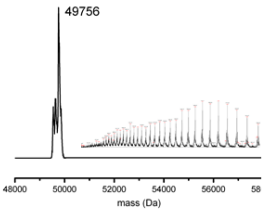

EGFP-Rab1bD53C-CC

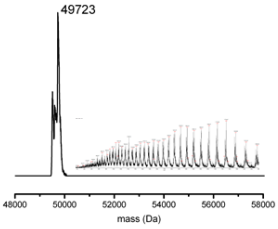

protein	calculated	observed
EGFP-Rab1bT34C-TF3-CC	50405	50395 (Δ=-10)
EGFP-Rab1bT34C_Q67L-TF3-CC	50390	50373 (Δ= -17)
EGFP-Rab1bS36C-TF3-CC	50419	50408 (Δ= -14)

Tide Fluor™ 3 maleimide [TF3 maleimide] M = 651.71 g/mol

protein	calculated	observed
EGFP-Rab1bT34C-CC	49754	49735 (Δ= -19)
EGFP-Rab1bS36C-CC	49768	49756 (Δ= -12)
EGFP-Rab1bD53C-CC	49740	49723 (Δ= -17)

-CC M = 224 g/mol

EGFP-K-RasD30C-MESNA **+TF3**

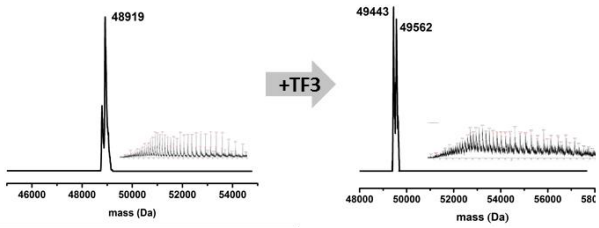

mCitrine-K-RasE31C-MESNA **+TF4**

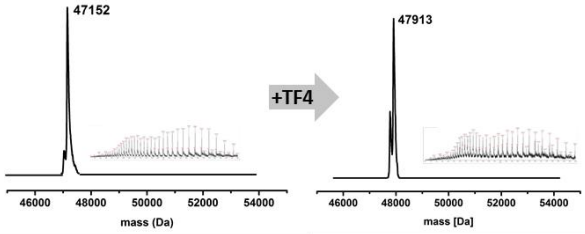

mCitrine-K-RasD30C-MESNA **+TF4**

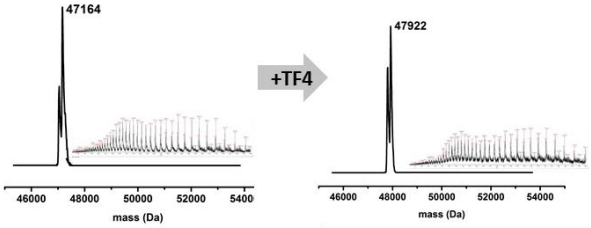

protein-TF3/TF4	calculated	observed
mCitrine-K-RasD30C-MESNA	47177	47164 (Δ= -13)
mCitrine-K-RasD30C-TF4-MESNA	47933	47922 (Δ=-11)
mCitrine-K-RasE31C-MESNA	47163	47152 (Δ=-11)
mCitrine-K-RasE31C-TF4-MESNA	47919	47913 (Δ=-6)

protein	calculated	observed
EGFP-K-RasD30C-MESNA	48933	48919 (Δ= -14)
EGFP-K-RasD30C-TF3-MESNA	49583	49562 (Δ= -21)

Tide Fluor™ 3 maleimide [TF3 maleimide] M = 651.71 g/mo
Tide Fluor™ 4 maleimide [T43 maleimide] M = 755.86 g/mol

EGFP-KRasD30C-TF3-CVIM

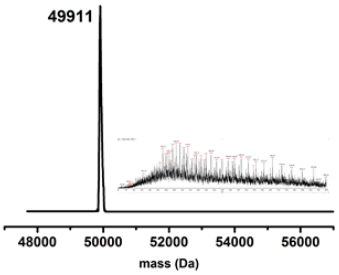

mCitrine-KRasD30C-TF4-CVIM

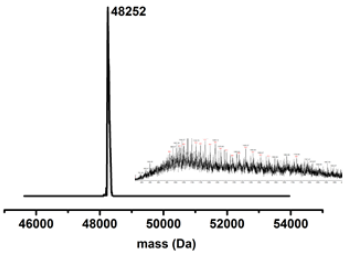

mCitrine-KRasE31C-TF4-CVIM

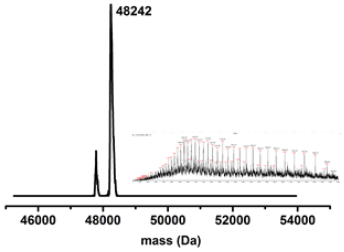

protein	calculated	observed
EGFP-K-RasD30C-TF3-CVIM	49904	49911 (Δ=+6)
mCitrine-K-RasD30C-TF4-CVIM	48253	48252 (Δ= -1)
mCitrine-K-RasE31C-TF4-CVIM	48239	48242 (Δ= +3)

Tide Fluor™ 3 maleimide [TF3 maleimide] M = 651.71 g/mol
Tide Fluor™ 4 maleimide [T43 maleimide] M = 755.86 g/mol

-CVIM M = 464.2 g/mol

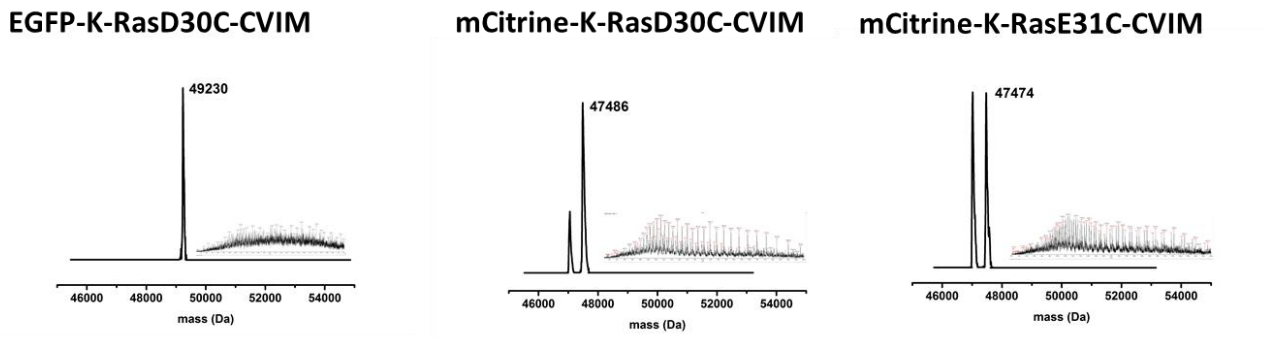

protein	calculated	observed
EGFP-K-RasD30C-CVIM	49254	49230 (Δ= -24)
mCitrine-K-RasD30C-CVIM	47498	47486 (Δ= -12)
mCitrineD11-K-Ras-E31C-CVIM	47484	47473 (Δ= -11)

-CVIM M = 464.2 g/mol

Figure S4 Electrospray ionization (ESI)-Mass Spectra of Rab1 and K-Ras constructs.

LC-ESI-MS measurements were performed on a Finnigan LCQ Advantage Max mass spectrometer (Finnigan, San Jose USA) coupled with an Agilent 1100 Series HPLC system (Agilent Technologies Inc.) equipped with a Grace Vydac 214TP C4-HPLC column (Thermo Fischer Scientific). Sample separation and desalting was achieved by elution from the HPLC column with a gradient of 20 % to 80 % acetonitrile with 0.08 % (v/v) TFA against aqueous buffer with 0.1 % (v/v) TFA. Data analysis and deconvolution was carried out by using the analysis software Xcalibur (Thermo Electron) and MagTran (Zhongqi Zhang, Amgen).

Supplementary Figure S5 Native chemical ligation (NCL)

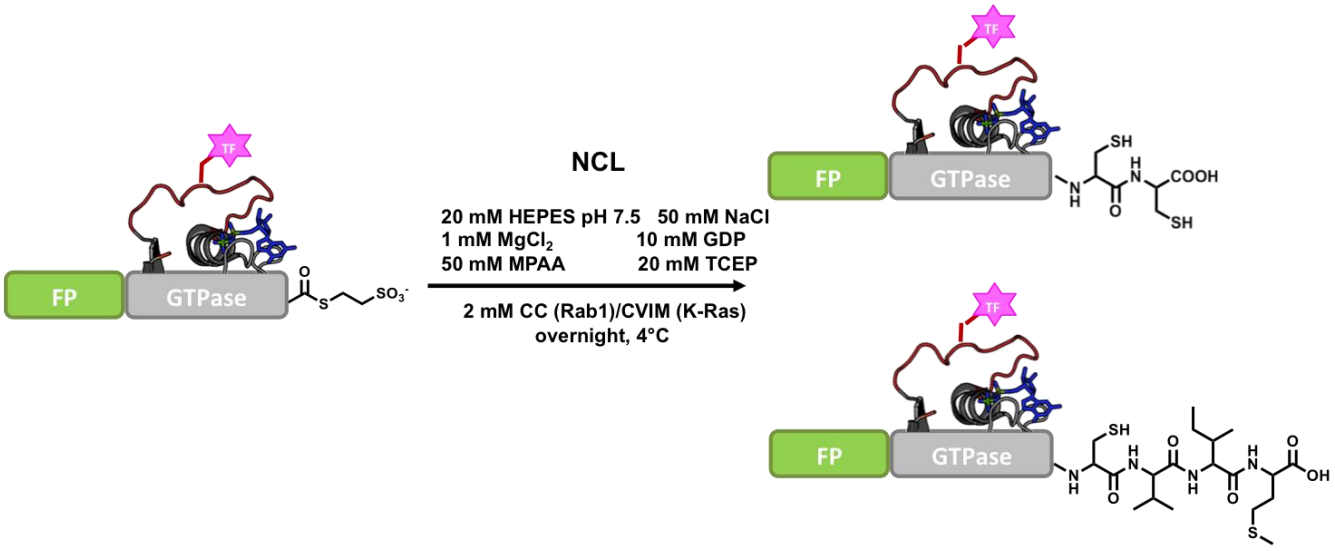

Figure S5 Scheme of NCL to reconstitute C-terminal prenylatable cysteines (CC motif for Rab1 and CVIM motif for K-Ras).

Supplementary Figure S6 Specific signal for nucleotide exchange

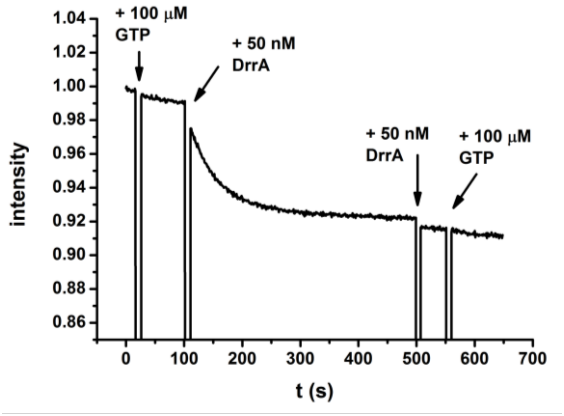

Figure S6 GEF-mediated nucleotide exchange.

Addition of the GEF domain DrrA$^{340\text{-}533}$ to 200 nM EGFP-Rab1bT34C-TF3 induces rapid nucleotide exchange in the presence excess GTP. After nucleotide exchange, further addition of GEF or GTP does not result in further change. FRET was monitored with excitation at 480 nm and emission at 580 nm.

Supplementary Figure S7 Specific signal for nucleotide exchange

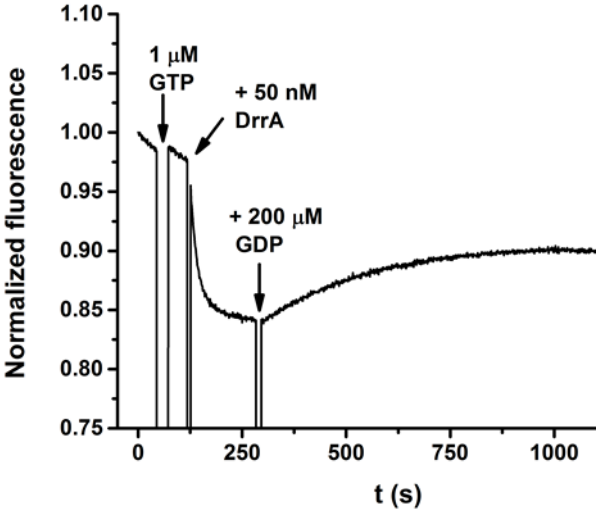

Figure S7 Reversibility of the nucleotide exchange.

After DrrA-mediated exchange of GTP for bound GDP in EGFP-Rab1bT34C-TF3, further addition of excess GDP reverses the process. FRET was monitored with excitation at 480 nm and emission at 580 nm.

Supplementary Figure S8

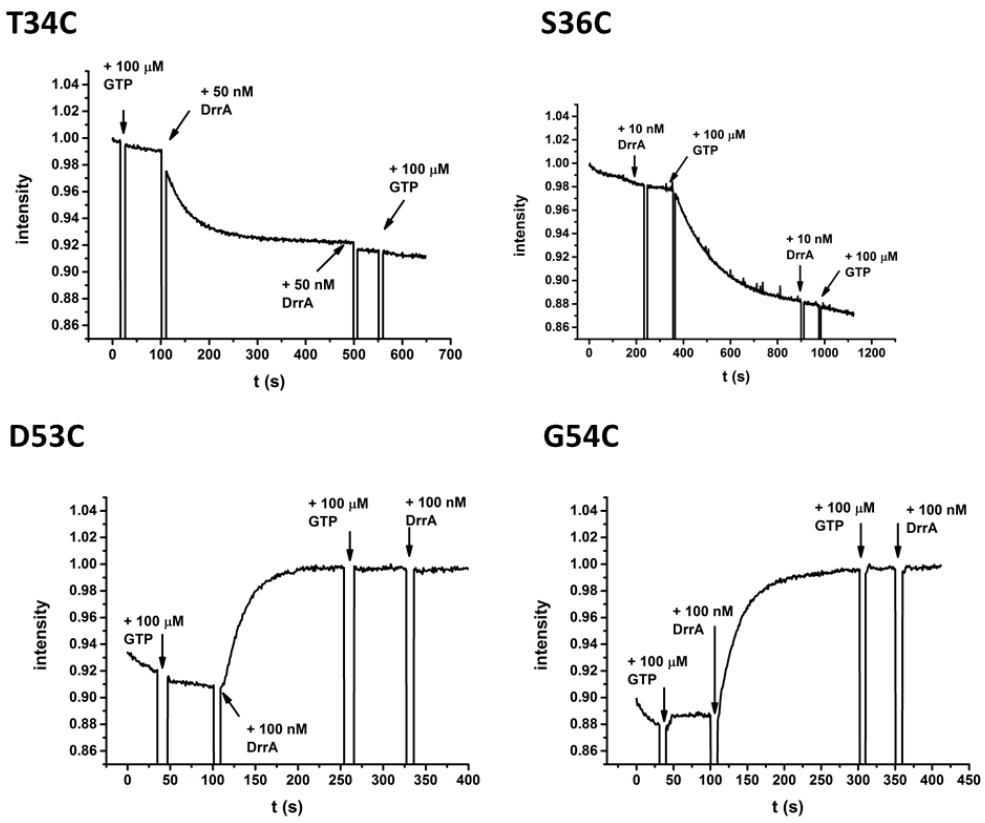

Figure S8 FRET change in Rab1 constructs upon nucleotide exchange

Addition of the GEF domain DrrA$^{340\text{-}533}$ to 200 nM EGFP-Rab1-TF3 constructs induces rapid nucleotide exchange in the presence excess GTP. After nucleotide exchange, addition of GEF or GTP does not result in further signal change. FRET was monitored with excitation at 480 nm and emission at 580 nm.

Supplementary Figure S9 Rate constants for Rab1 nucleotide exchange

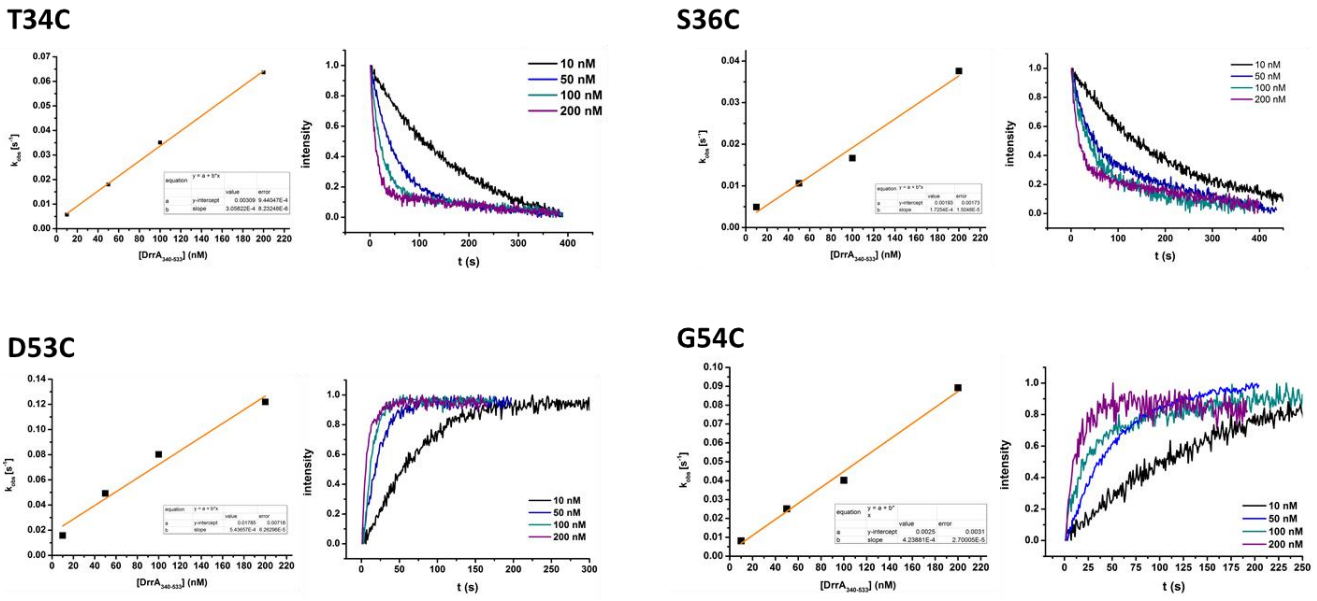

Figure S9 Second-order rate constants of GEF-mediated nucleotide exchange of Rab1 constructs.

Observed rate constants for nucleotide exchange mediated by DrrA$^{340\text{-}533}$ (10, 50, 100 and 200 nM) in the presence of 100 μM GTP are plotted against DrrA concentration. FRET was monitored with excitation at 480 nm and emission at 580 nm.

Supplementary Figure S10 GAP assay

T34C

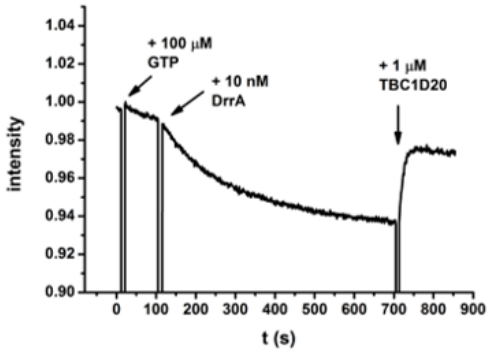

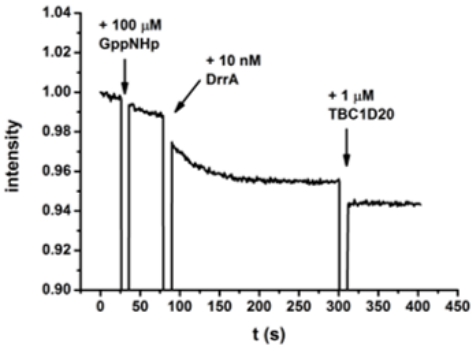

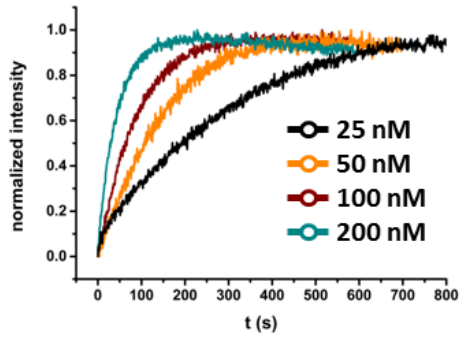

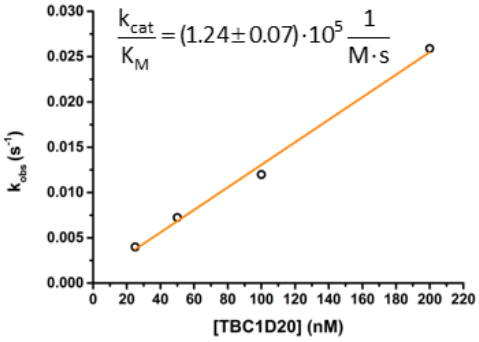

S36C

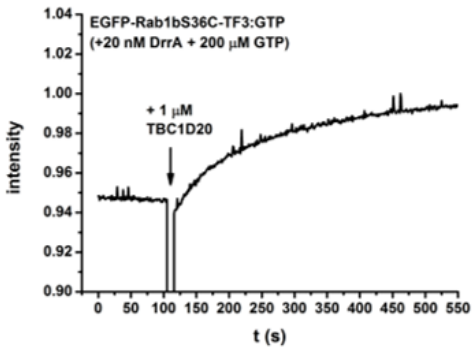

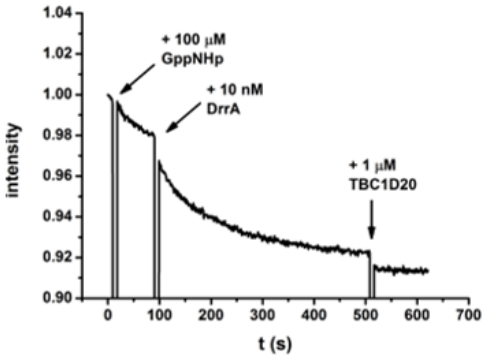

D53C

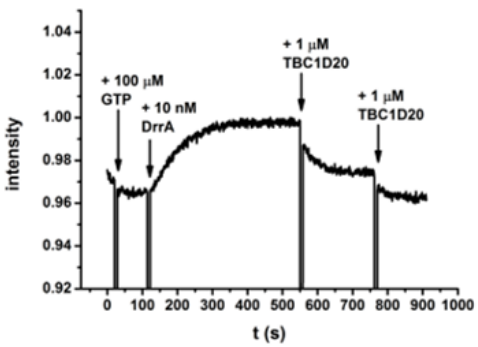

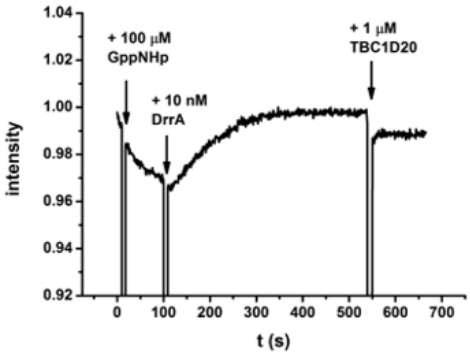

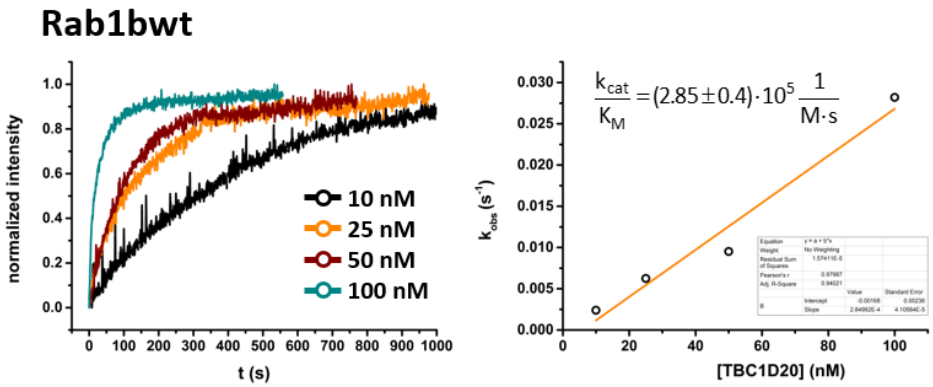

Figure S10 TBC1D20 induces bound GTP hydrolysis but not for bound GppNHp.

GAP-induced GTP hydrolysis was observed through addition of 25 nM-2 µM TBC1D20$^{1-362}$ to 200 nM Rab1 constructs after GDP/GTP exchange. When GppNHp is used, TBC1D20$^{1-362}$ failed to reverse the FRET signal change. FRET was monitored with excitation at 480 nm and emission at 580 nm. For the T34C construct and Rab1b wt, the GAP catalytic efficiencies were determined through addition of 10-200 nM TBC1D20$^{1-362}$ to 1 µM GTP:EGFP-Rab1bT34C-TF3 or mantGTP:Rabwt. The change in FRET for GTP:EGFP-Rab1bT34C-TF3 was monitored with excitation at 480 nm and emission at 580 nm. The change in mantGTP upon GTP hydrolysis was monitored with excitation at 360 nm and emission at 438 nm.

Supplementary Figure S11 OCRL binding

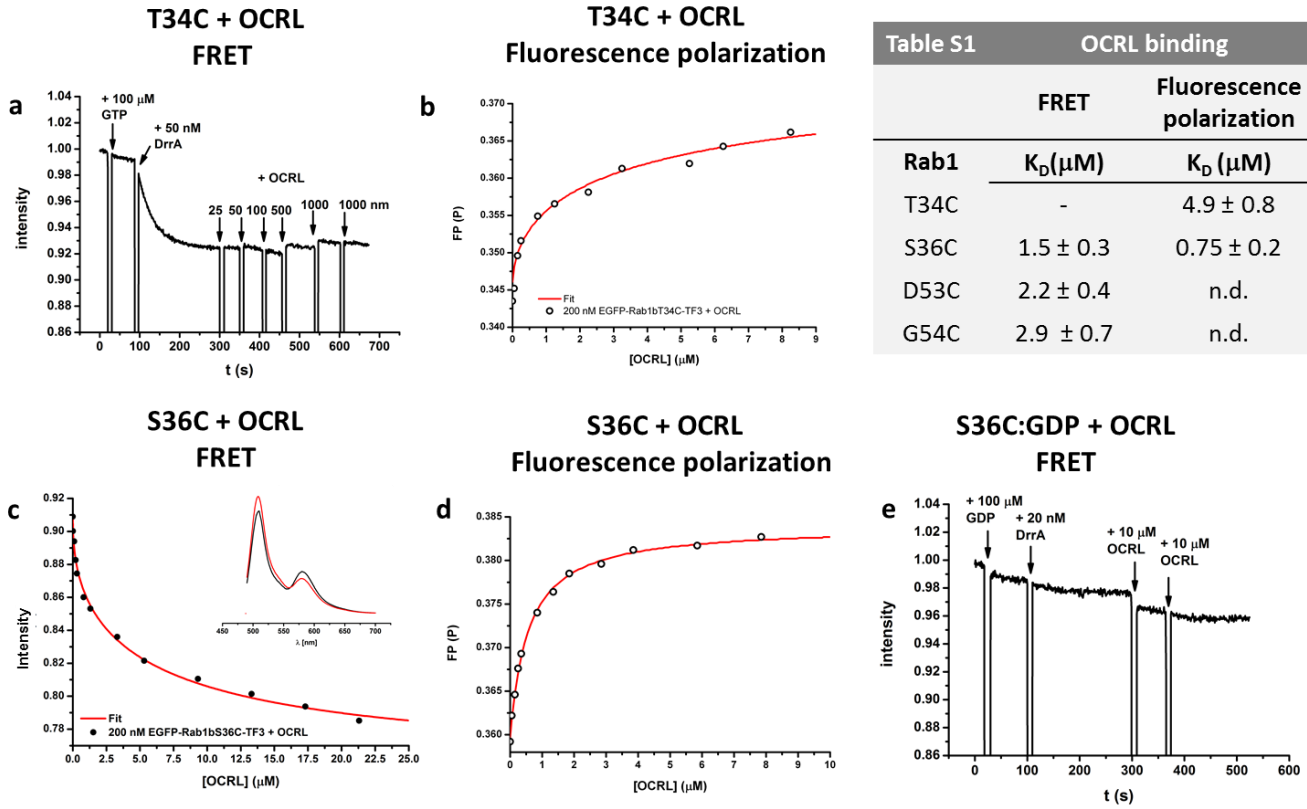

Table S1	OCRL binding	
	FRET	Fluorescence polarization
Rab1	K_D(µM)	K_D (µM)
T34C	-	4.9 ± 0.8
S36C	1.5 ± 0.3	0.75 ± 0.2
D53C	2.2 ± 0.4	n.d.
G54C	2.9 ± 0.7	n.d.

Figure S11 Binding of OCRL to Rab1 constructs.

OCRL1$^{539–901}$ was titrated to **(a)** 200 nM GTP-bound EGFP-Rab1bT34C-TF3, **(c)** 200 nM GTP-bound EGFP-Rab1bS36C-TF3 and **(e)** 200 nM GDP-bound EGFP-Rab1bS36C-TF3. FRET was monitored with excitation at 480 nm and emission at 580 nm. **(c inset)** Fluorescence spectra of EGFP-Rab1bS36C-TF3 before (black line) and after binding to OCRL (red line). **(b, d)** OCRL binding was independently measured by fluorescence polarization.

Dissociation constant K_D was obtained by fitting to a quadratic equation as described previously[3,4].

Table S1 Summary of OCRL binding dissociation constants (K_D) for Rab1 constructs. Errors represent fitting errors

Supplementary Figure S12 LidA binding

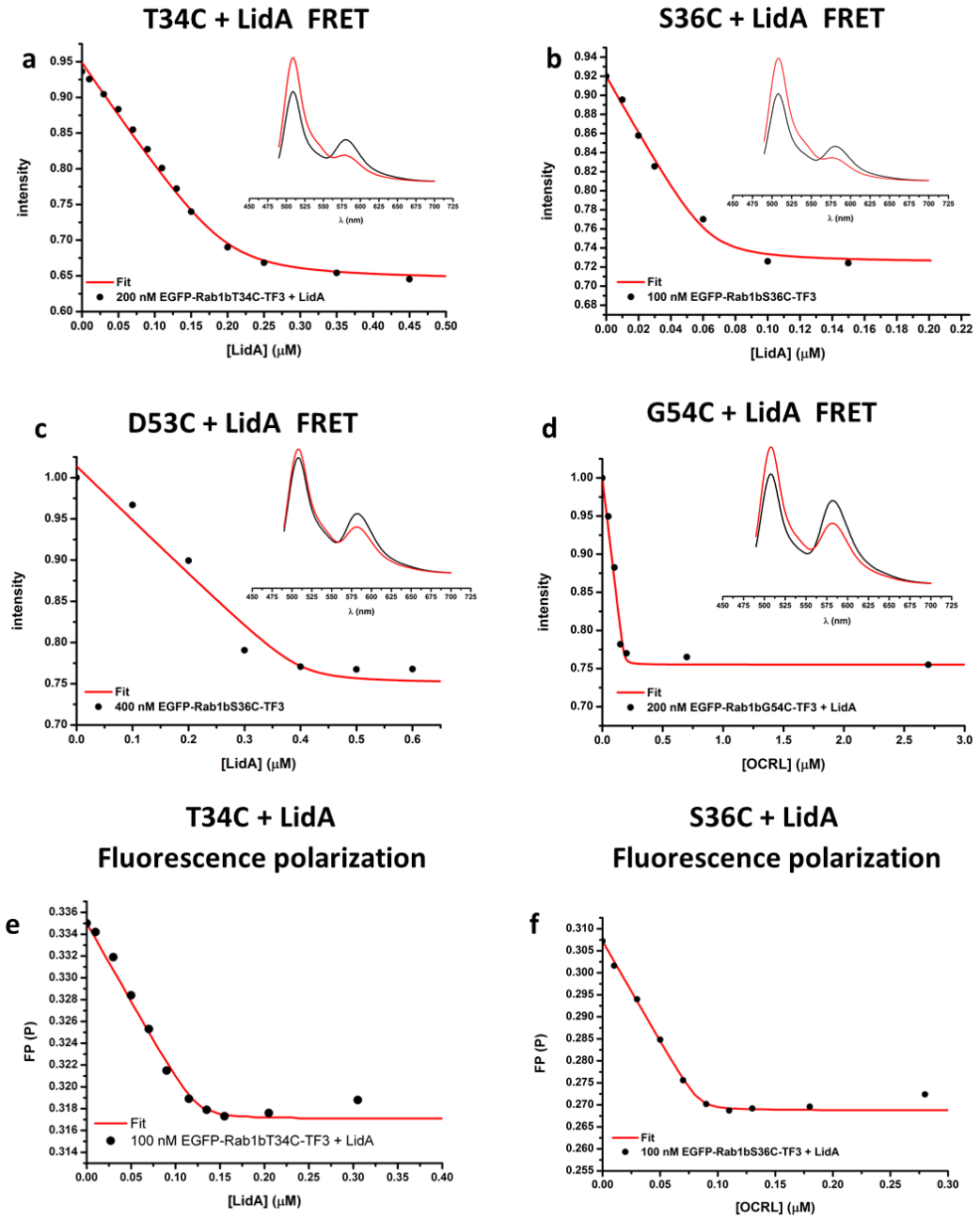

Table S2	LidA binding	
	FRET	Fluorescence polarization
Rab1	K_D(μM)	K_D (μM)
T34C	< 10 nM	< 10 nM
S36C	< 10 nM	< 10 nM
D53C	< 10 nM	n.d.
G54C	< 10 nM	n.d.

Figure S12 Binding of LidA to Rab1 constructs.

LidA$^{201-583}$ was titrated to GTP-bound **(a)** EGFP-Rab1bT34C-TF3, **(b)** EGFP-Rab1bS36C-TF3, **(c)** EGFP-Rab1bD53C-TF3 and **(d)** EGFP-Rab1bG54C-TF3. **Insets:** Fluorescence spectra of EGFP-Rab1b-TF3 constructs before (black line) and after binding to LidA (red line). FRET was monitored with excitation at 480 nm and emission at 580 nm. **(e, f)** LidA binding was independently measured by fluorescence polarization with excitation at 480 nm and emission at 510 nm.

Table S2 Summary of LidA binding dissociation constants (K_D) for Rab1 constructs. Errors represent fitting errors

Supplementary Figure S13 LidA binding to GDP-bound Rab1

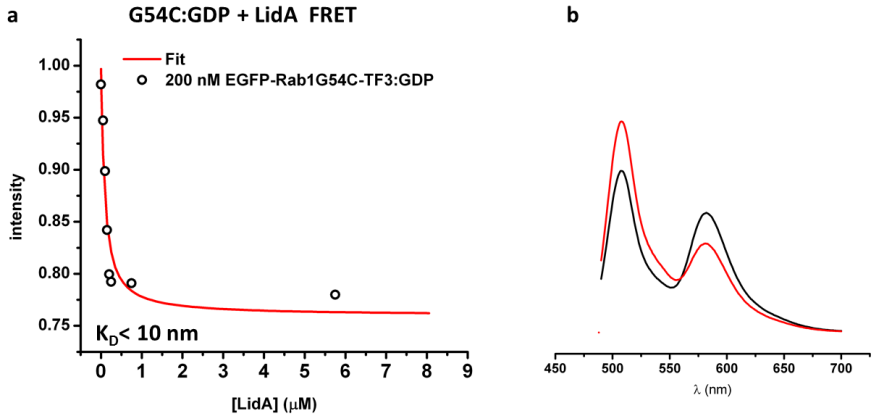

Figure S13 LidA binding to GDP-bound Rab1

(a) LidA$^{201-583}$ was titrated to GDP-bound EGFP-Rab1bG54C-TF3. FRET was monitored with excitation at 480 nm and emission at 580 nm. **(b)** Fluorescence spectra of GDP-bound EGFP-Rab1bG54C-TF3 before (black line) and after binding to LidA (red line).

Supplementary Figure S14 Sensor immobilization

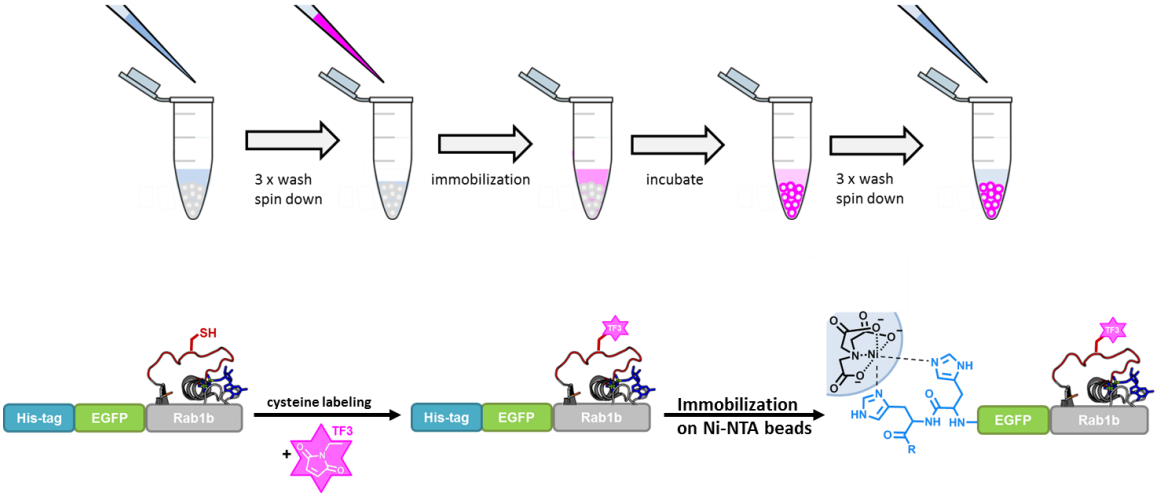

Figure S14 Scheme for immobilization of Rab1 sensors on Ni-NTA beads

For immobilization of the Rab1 sensor constructs, 50 µl of Ni-NTA beads were washed by suspending the beads in 500 µl GTPase buffer (20 mM HEPES pH 7.5, 20 mM NaCl, 2 mM DTE, 1 mM $MgCl_2$). Spin them down with a centrifuge and remove the supernatant. Repeat the process with fresh buffer for three times. 20 µl of the protein solution was added to 10 µl of the suspended beads and incubated for 30-60 min. After incubation the suspension was spinned down, the supernatant was removed and the beads were washed twice with 200 µl fresh GTPase buffer. Finally 20-50 µl of the beads suspension was transferred onto object slide and imaged by FLIM through a 40x/1.35 UPlanSApo air objective.

Supplementary Figure S15 Ni-NTA beads – donor only control

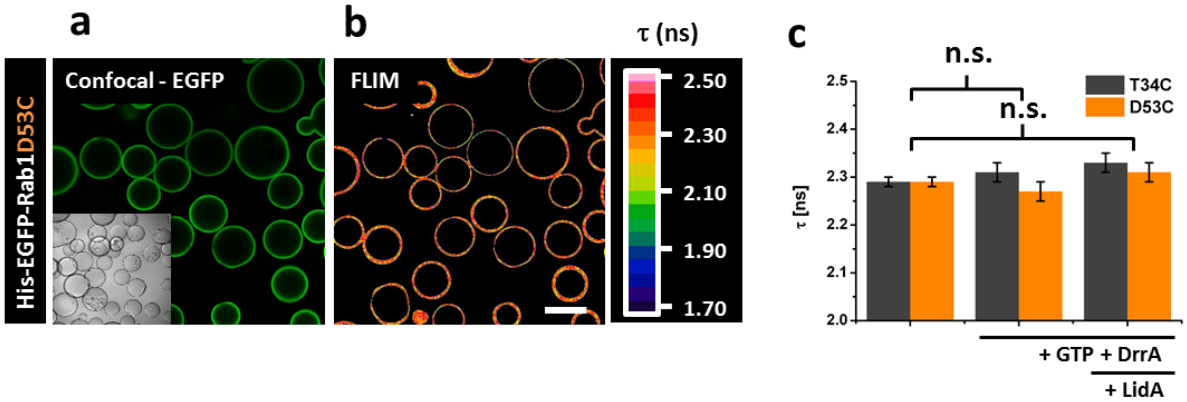

Figure S15 Ni-NTA beads – donor only control

(a) Fluorescence and **(b)** FLIM image of GDP-bound His-EGFP-Rab1D53C immobilized on Ni-NTA beads. **(c)** Quantification of EGFP fluorescence lifetime of Rab1 constructs on the beads incubated with 100 µM GDP, 100 µM GTP + 1 µM DrrA and 100 µM GTP + 1 µM DrrA + 1 µM LidA, respectively,

(n = 5 images with > 15 beads, mean ± s.d., two-tailed t-test, P > 0.2 not significant); Scale bar: 100 µm.

Supplementary Figure S16 Cellular localization of Rab1 sensor

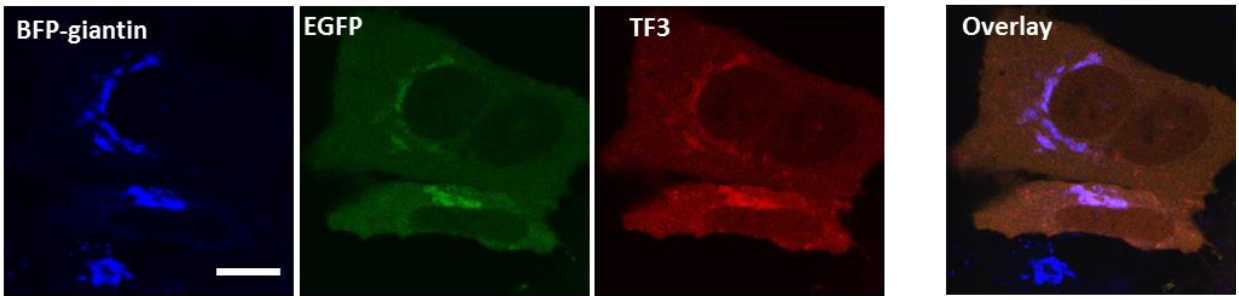

Figure S16 EGFP-Rab1T34C-TF3-CC localizes at the Golgi apparatus correctly.

Fluorescence images of EGFP-Rab1T34C-TF3-CC microinjected into HeLa cells expressing Golgi marker, BFP-Giantin. Scale bar: 10 µm.

Supplementary Figure S17 Dynamics of Rab1 sensor in the live cell

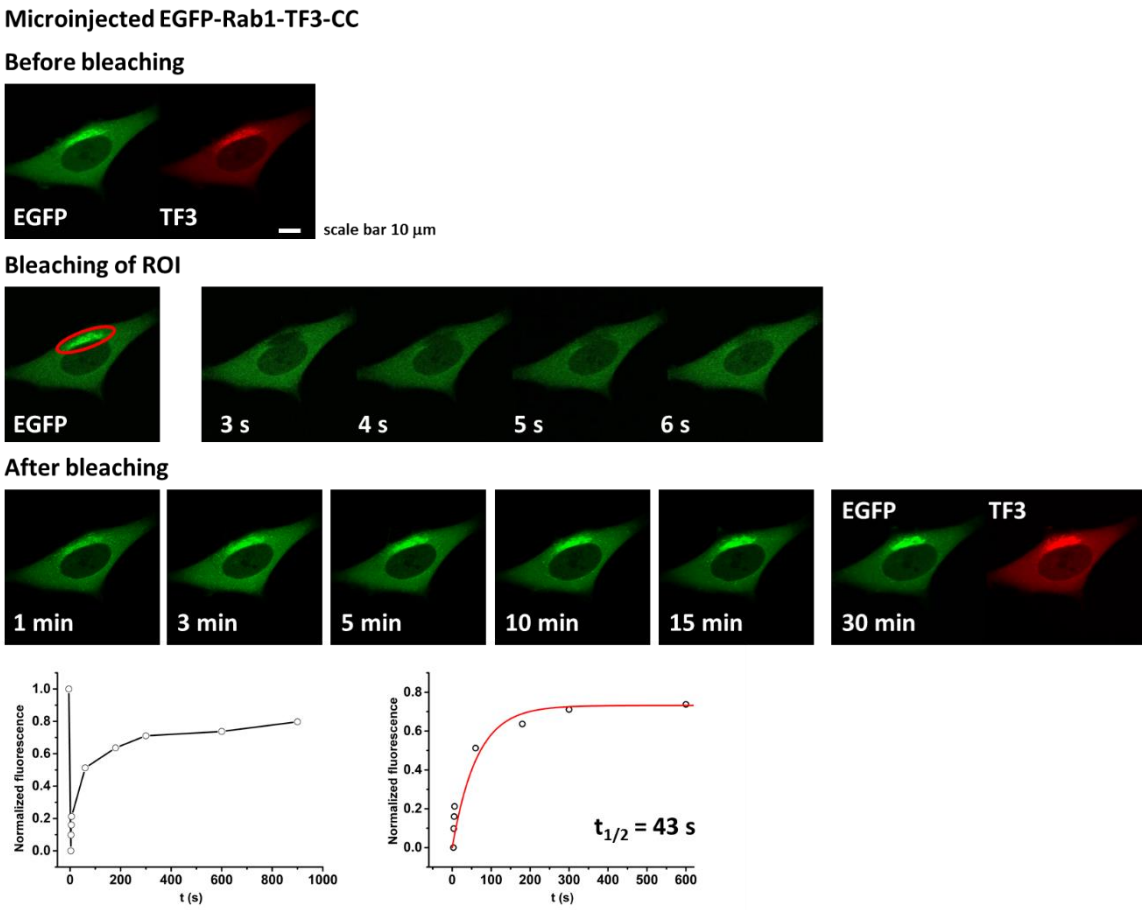

Figure S17 Fluorescence Recovery After Photobleaching (FRAP) measurement of EGFP-Rab1-TF3-CC construct in the live cell. EGFP was bleached at the Golgi region. After bleaching the EGFP fluorescence recovers over time at the Golgi.

Supplementary Figure S18 Nucleotide binding state in the cell

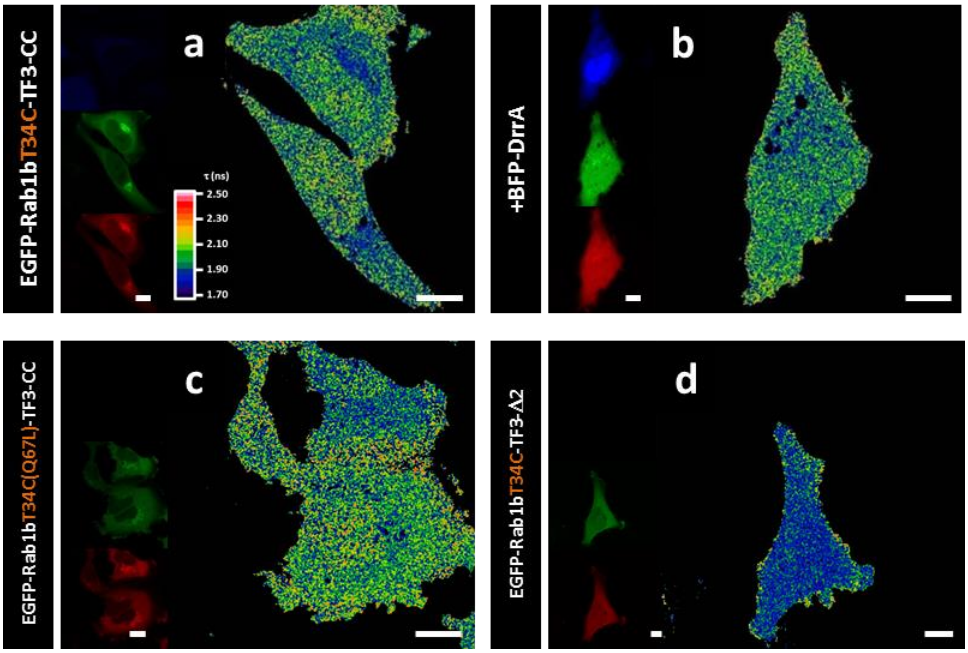

Figure S18 FLIM measurements of Rab1 nucleotide binding state in the cell.

(a) FLIM images of EGFP-Rab1T34C-TF3-CC in HeLa cells and **(b)** HeLa cells expressing BFP-DrrA$^{340-533}$. **(c)** FLIM images of EGFP-Rab1(Q67L)T34C-TF3-CC and **(d)** EGFP-Rab1T34C-TF3-Δ2 in HeLa cells. Confocal images were shown in the left. Scale bars: 10 µm.

Supplementary Figure S19 Quantification of nucleotide binding state

The relative amount of GDP and GTP-bound Rab1 were obtained from the lifetime images of the COSGA sensor using the following relations:

In the FLIM images each color coded pixel correlates to a specific lifetime that is determined through the collected photons at a specific position, e.g. in the cytoplasm or at the Golgi. The average lifetime at this position (τ_{av}) is composed of two fractions. One fraction represents the GDP-bound status and the other fraction correlates with the lifetime of the GTP-bound status. (see below Eq. 1)

Eq. 1 $\tau_{av} = x * \tau_{GTP} + y * \tau_{GDP}$ with $x + y = 1$

Here τ_{av} is the lifetime of the FRET sensor at a specific location in the cell. x represents the fraction of GTP-bound sensor and y for the fraction of GDP-bound sensor. τ_{GDP} and τ_{GTP} are the lifetimes of GDP- and GTP-bound species, respectively.

τ_{GDP} and τ_{GTP} were determined independently in control experiments using GDP-bound and GTP-bound sensors, as described in the main text. For the GDP-bound sensor (here the Rab1T34CΔ2 construct lacking the C-terminal prenylatable cysteines) the lifetime was determined as τ_{GDP} = 1.88 ns. For the GTP-bound sensor (here the constitutively active Rab1T34C(Q67L) mutant or expression of BFP-DrrA$^{340-533}$) the lifetime was determined as τ_{GDP} = 2.05 ns.

Through rearrangement of Eq. 1 we can translate the fluorescence lifetime into the percentage of active GTP-bound (x) or inactive GDP-bound (y) for each measurement, leading to Fig 4e.

$\rightarrow x = \frac{\tau_{av}-\tau_{GDP}}{\tau_{GTP}-\tau_{GDP}}$ $y = \frac{\tau_{GTP}-\tau_{av}}{\tau_{GTP}-\tau_{GDP}}$ with τ_{GDP} = 1.88 ns and τ_{GDP} = 2.05 ns

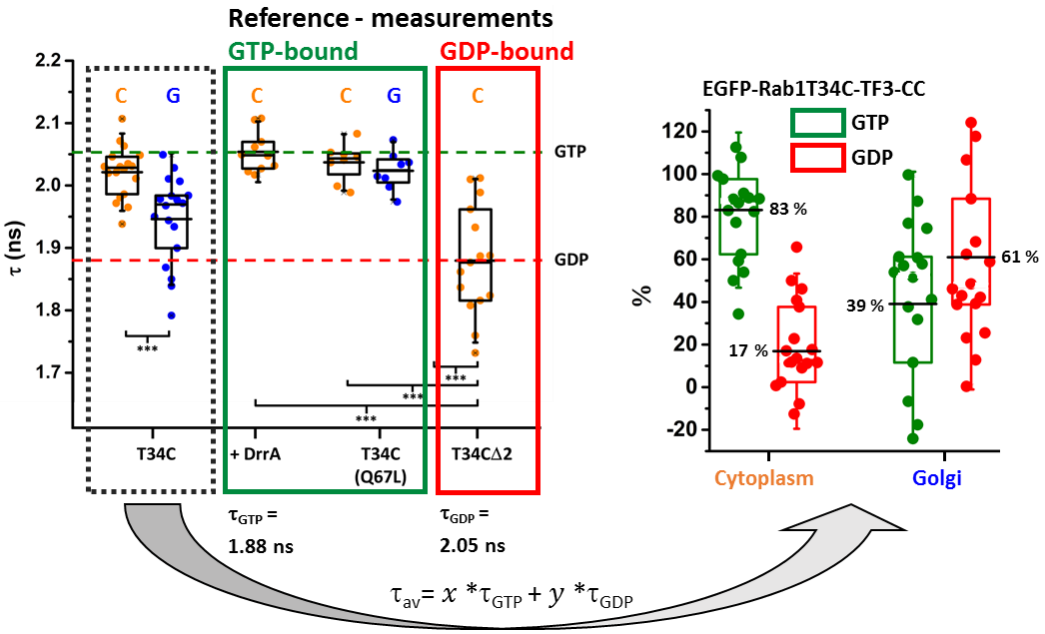

Figure S19 Quantification of nucleotide binding state of Rab1 at the cytoplasm and Golgi.

Supplementary Figure S20 Structural alignment of Rab1 with K-Ras

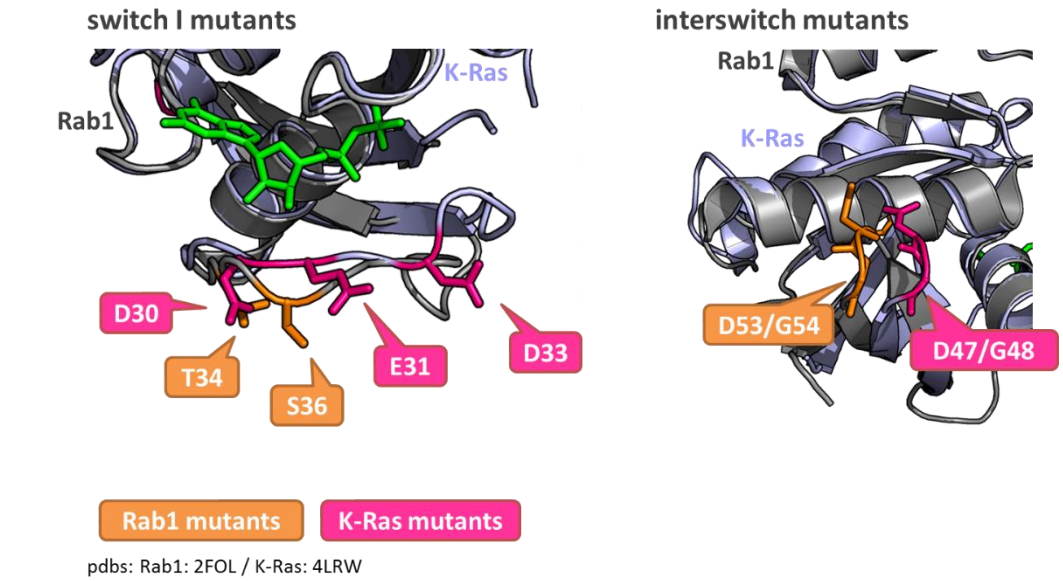

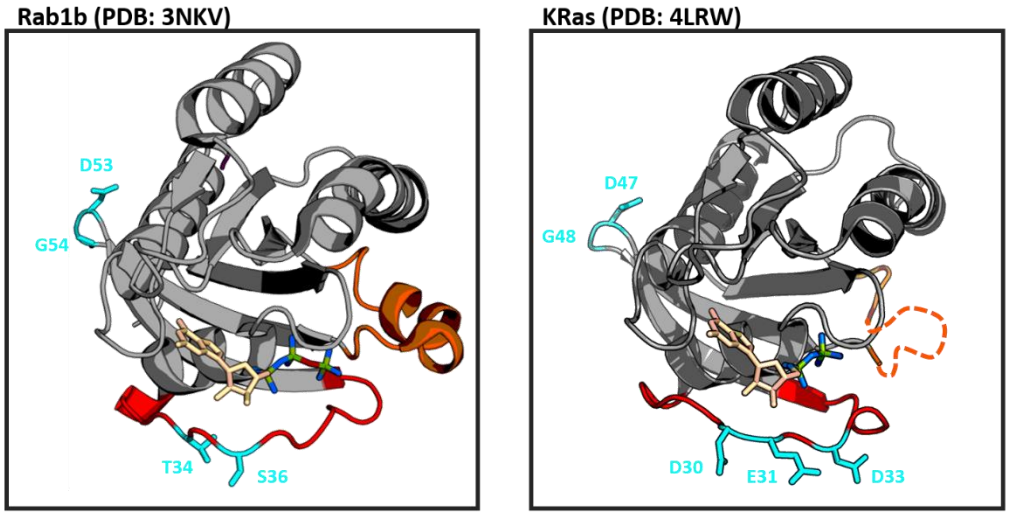

Figure S20 Structural alignment of Rab1 with K-Ras to identify labeling site on K-Ras.

Supplementary Figure S21 GEF assay using mantGDP

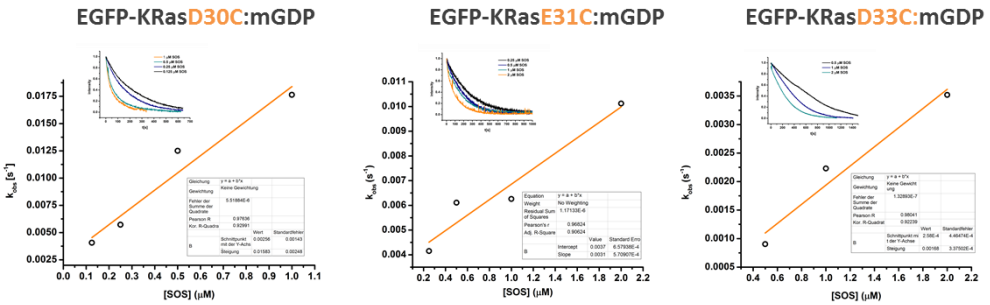

Table S3	SOS
K-Ras	k_{cat}/K_M $(M \cdot s)^{-1}$
D30C	$(1.58 \pm 0.25) \times 10^4$
E31C	$(0.31 \pm 0.06) \times 10^4$
D33C	$(0.17 \pm 0.04) \times 10^4$
D47C	$(0.59 \pm 0.08) \times 10^4$
G48C	$(8.38 \pm 0.07) \times 10^4$
E107C	$(0.21 \pm 0.01) \times 10^4$
wt	$(5.23 \pm 0.03) \times 10^4$

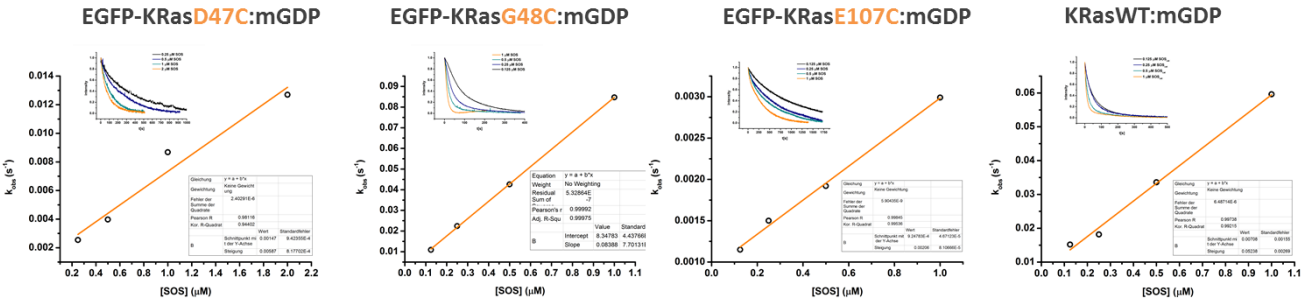

Figure S21 GEF assay for K-Ras constructs using mantGDP.

Observed rate constants for nucleotide exchange mediated by SOS^{cat} in the presence of 100 µM GTP are plotted against SOS^{cat} concentration. **Table S3** Summary of second-order rate constants (k_{cat}/K_M) for K-Ras constructs. Errors represent fitting errors. MantGDP release upon nucleotide exchange was monitored as the drop in Mant-fluorescence intensity with excitation set at 367 nm and emission at 439 nm.

Supplementary Figure S22 K-Ras sensor for nucleotide exchange

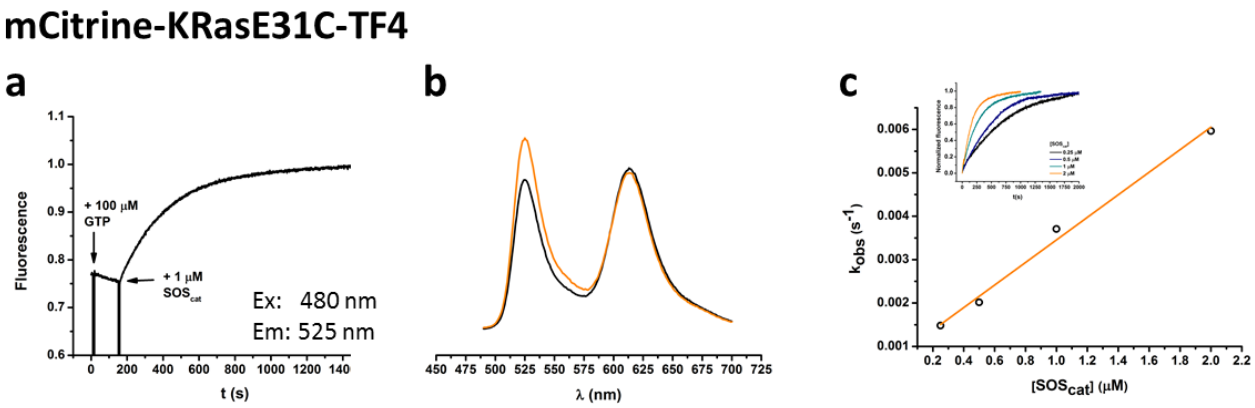

E31C	SOS
signal	k_{cat}/K_M $(M \cdot s)^{-1}$
mCitrine-TF4	$(0.26 \pm 0.02) \times 10^4$

Figure S22 GEF-mediated nucleotide exchange in mCitrine-KRasE31C-TF4.

(a) Addition of the GEF domain SOS^{cat} to 200 nM mCitrine-KRasE31C-TF4 induces rapid nucleotide exchange in the presence of excess GTP (100 µM). FRET was monitored as increase in donor fluorescence (corresponding to decrease in FRET) with excitation at 480 nm and emission at 525 nm. **(b)** Fluorescence spectra of mCitrine-KRasE31C-TF4 constructs before (black line) and after nucleotide exchange (orange line). **(c)** Observed rate constants for nucleotide exchange mediated by SOS^{cat} in the presence of 100 µM GTP are plotted against SOS^{cat} concentration, yielding the second-order rate constant (k_{cat}/K_m) shown in the table. Errors represent fitting errors.

Supplementary Figure S23 K-Ras sensor for GAP assay

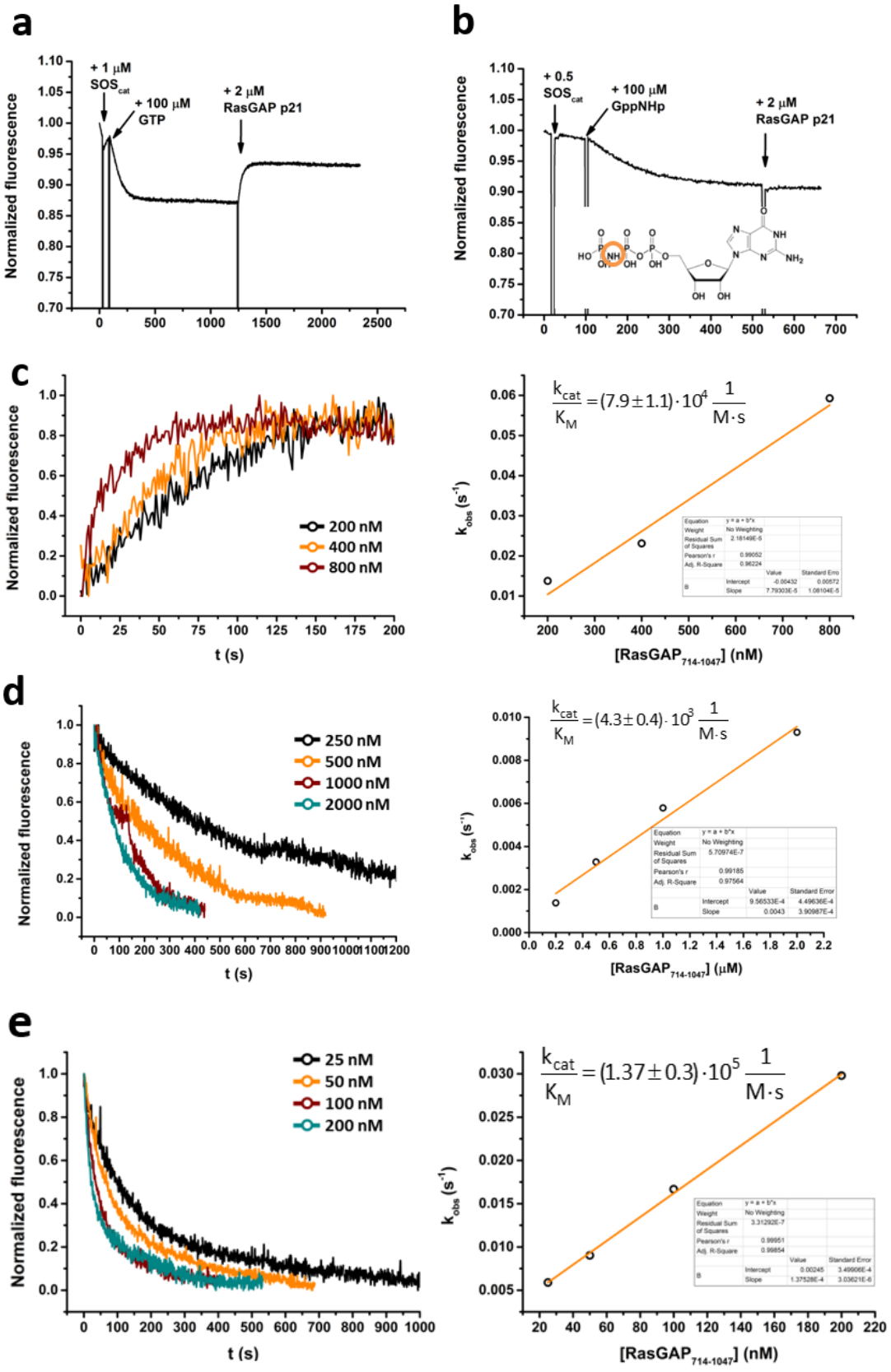

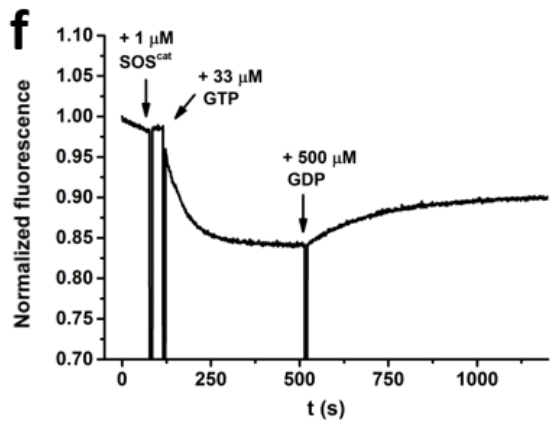

Figure S23 RasGAP induces GTP hydrolysis.

(a) GAP-induced GTP hydrolysis was observed through addition of 2 μM RasGAP$^{714\text{-}1047}$ to 200 nM EGFP-KRasD30C-TF3 after exchange of GTP for GDP. **(b)** When GppNHp was used, RasGAP$^{714\text{-}1047}$ failed to reverse the FRET signal change. For **(c)** EGFP-K-RasD30C-TF3 and **(d)** mCitrineD11-K-RasE31C-TF4, the catalytic efficiencies of RasGAP$^{714\text{-}1047}$-induced GTP hydrolysis were determined by addition of 0.2-2 μM RasGAP$^{714\text{-}1047}$ to GTP:EGFP-K-RasD30C-TF3 or GTP:mCitrineD11-K-RasE31C-TF4. The change in FRET for EGFP-K-RasD30C-TF3 was monitored with excitation at 480 nm and emission at 580 nm. The change in FRET for mCitrineD11-K-RasE31C-TF4 was monitored with excitation at 480 nm and emission at 525 nm. **(e) T**he catalytic efficiency of RasGAP$^{714\text{-}1047}$ towards K-Raswt was determined by addition of 25-200 nM RasGAP$^{714\text{-}1047}$ to 1 μM mantGTP:K-Ras wt. The change in mantGTP upon GTP hydrolysis was monitored with excitation at 360 nm and emission at 438 nm. **(f)** Addition of the GEF domain SOS^{cat} to 200 nM EGFP-KRasD30C-TF3 induces rapid nucleotide exchange in the presence excess GTP. Further addition of excess GDP reverses the process. FRET was monitored with excitation at 480 nm and emission at 580 nm.

Supplementary Figure S24 Control with donor only

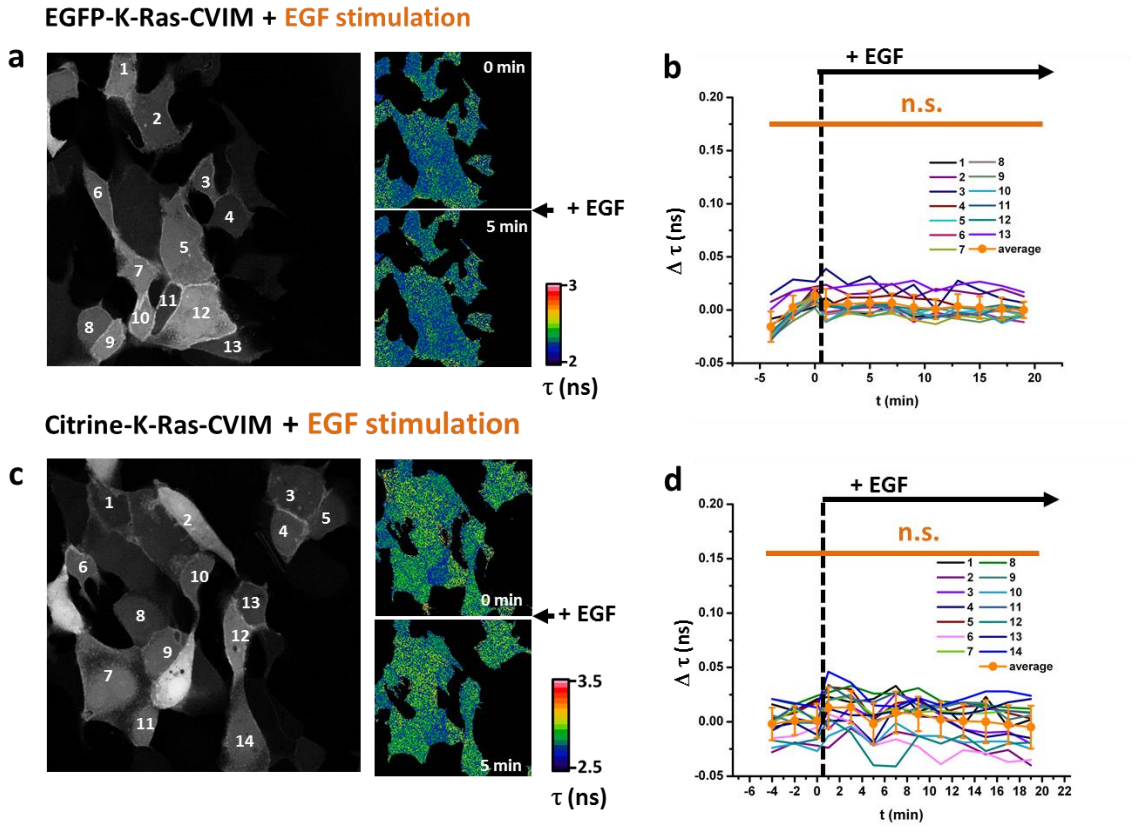

Figure S24 FLIM measurements of K-Ras constructs with donor only.

MDCK cells were microinjected with sensor constructs without acceptor dye, **(a)** EGFP-KRAS-CVIM and **(c)** mCitrine-KRas-CVIM. Upon EGF stimulation no significant change in donor lifetime was observed. Quantification of donor lifetime change of **(b)** EGFP-KRas-CVIM (orange line: mean ± s.d. (n=13 cells)) and **(d)** mCitrine-KRas-CVIM (orange line: mean ± s.d. (n=14 cells)). Colored lines represent individual cell profiles.

Supplementary Figure S25 Control without CAAX box

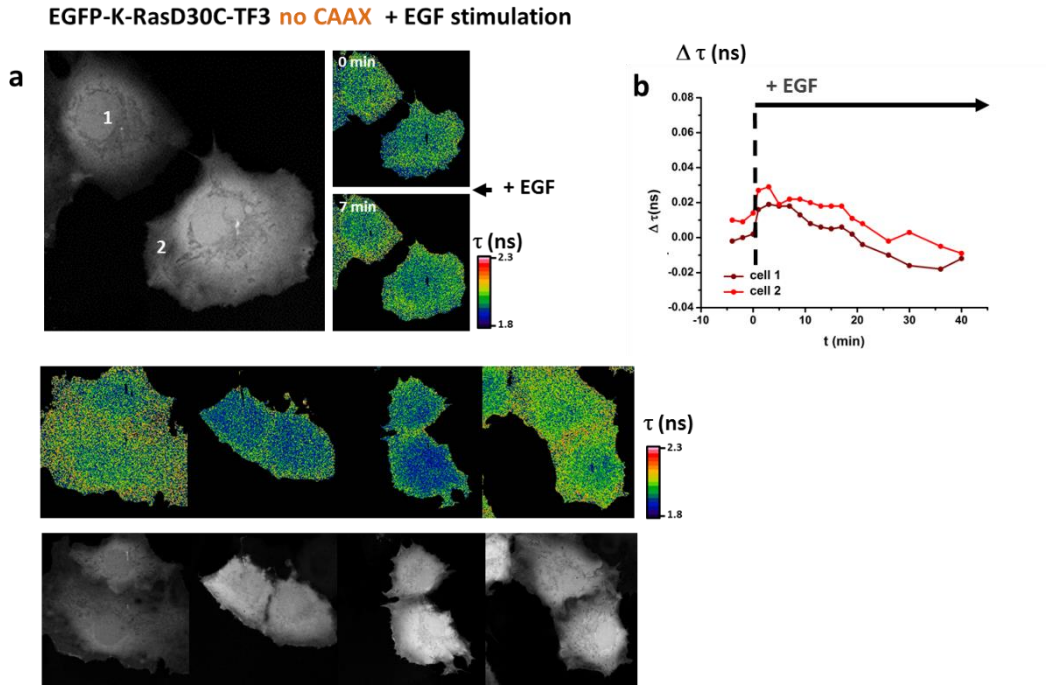

Figure S25 FLIM measurements of K-Ras constructs lacking C-terminal CAAX box.

(a) MDCK cells were microinjected with EGFP-KRasD30C-TF3 lacking the C-terminal CVIM motif. The protein cannot be prenylated and therefore is not functional. **(b)** Quantification of donor lifetime change. Upon EGF stimulation no significant change in donor lifetime was observed.

Supplementary Figure S26 Control with Erlontinib treatment

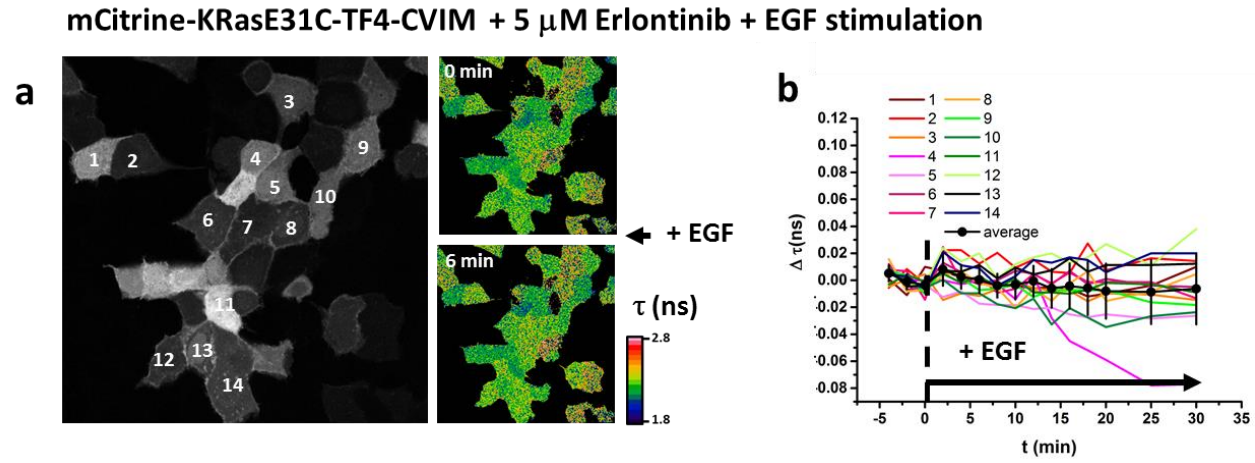

Figure S26 FLIM measurements of mCitrine-KRas-E31C-TF4-CVIM in the presence of Erlontinib.

(a) MDCK cells were treated with 5 μM Erlontinib 3 h prior to EGF stimulation[5,6]. **(b)** Quantification of donor lifetime change. Upon EGF stimulation no significant change in donor lifetime was observed. Colored lines represent individual cell profiles. (black line: mean ± s.d. (n=14 cells)).

Supplementary Figure S27 Dynamic range of K-Ras sensor

To correlate the FRET measurements by the sensitized emission with those by FLIM, we translate them into the FRET efficiency. For spectroscopic measurements, the FRET efficiency can be obtained from the change in donor intensity:

$$E_{FRET} = 1 - \frac{I_{DA}}{I_D}$$

where I_{DA} and I_D are the donor fluorescence intensities with and without an acceptor.

For fluorescence lifetime measurements, the FRET efficiency can be calculated using the following relation for the donor fluorescence lifetime:

$$E_{FRET} = 1 - \frac{\tau_{DA}}{\tau_D}$$

where τ_D and τ_{DA} are the donor fluorescence lifetimes with and without an acceptor.

We use EGFP-KRasD30C-TF3 as an example. Based on the FLIM measurements in the cell, the FRET efficiency can be obtained as

Before EGF stimulation: $E_{FRET} = 1 - \frac{2.01\,ns}{2.35\,ns} = 14.5\,\%$, after EGF stimulation: $\mathrm{E_{FRET}} = 1 - \frac{2.095\ \mathrm{ns}}{2.35\ \mathrm{ns}} = 10.9\,\%$

Based on the sensitized emission measurements in vitro, the FRET efficiency can be obtained as

Before adding SOS: $E_{FRET} = 1 - \frac{1.287}{2.405} = 46.5\,\%$, after adding SOS: $E_{FRET} = 1 - \frac{1{,}857}{2.405} = 22.7\,\%$

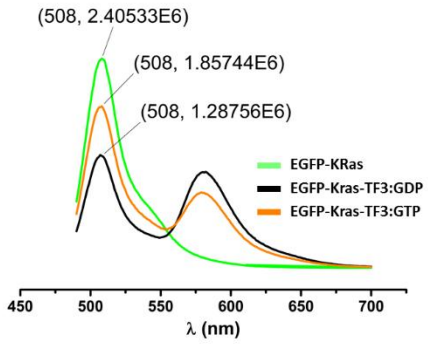

Figure S27 Emission scan of EGFP-KRasD30C (green line), EGFP-KRasD30C-TF3 before (black) and after (orange line) SOS-mediated nucleotide exchange.

Measurements by fluorescence lifetime in the cell and sensitized emission in vitro recorded a decrease of EFRET by 25% after EGF stimulation and by 51% after SOS-mediated GTP/GDP exchange, respectively. The in vitro measurement reveals the full dynamic range of the sensor, because in this

case GDP-bound K-Ras is quantitatively converted to GTP-bound K-Ras. The observed change in FRET efficiency is smaller in the cellular assay as in this case a mixture of GDP (e.g. cytosolic) and GTP-bound sensor is observed before and after activation resulting in a decreased observed dynamic range.

Supplementary Figure S28 Membrane ruffles

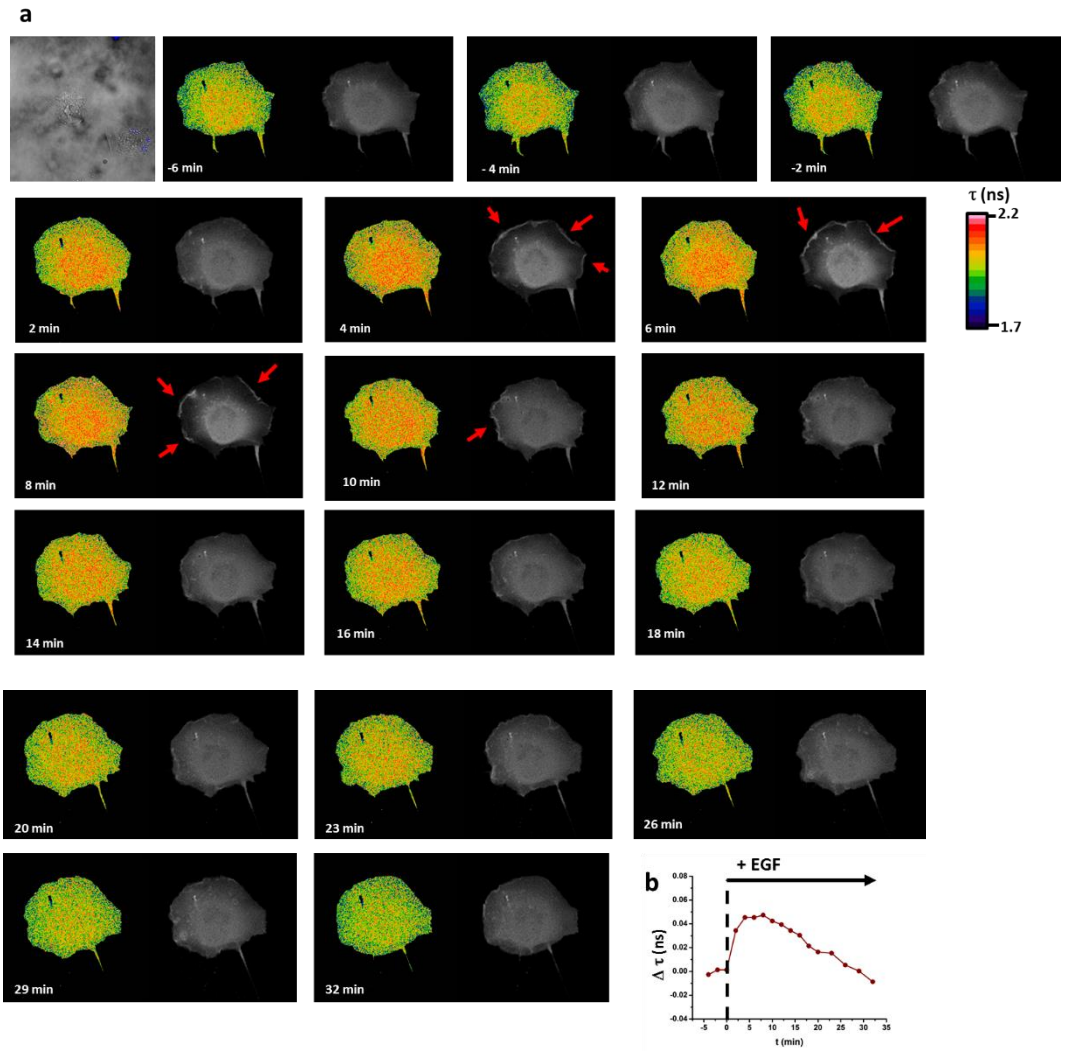

Figure S28 EGF induced membrane ruffles.

(a) Membrane ruffles are induced by EGF stimulation in COS-7 cells, as indicated by red arrows. **(b)** Quantification of donor lifetime change upon EGF stimulation.

Supplementary Figure S29 Rab1 cycling model

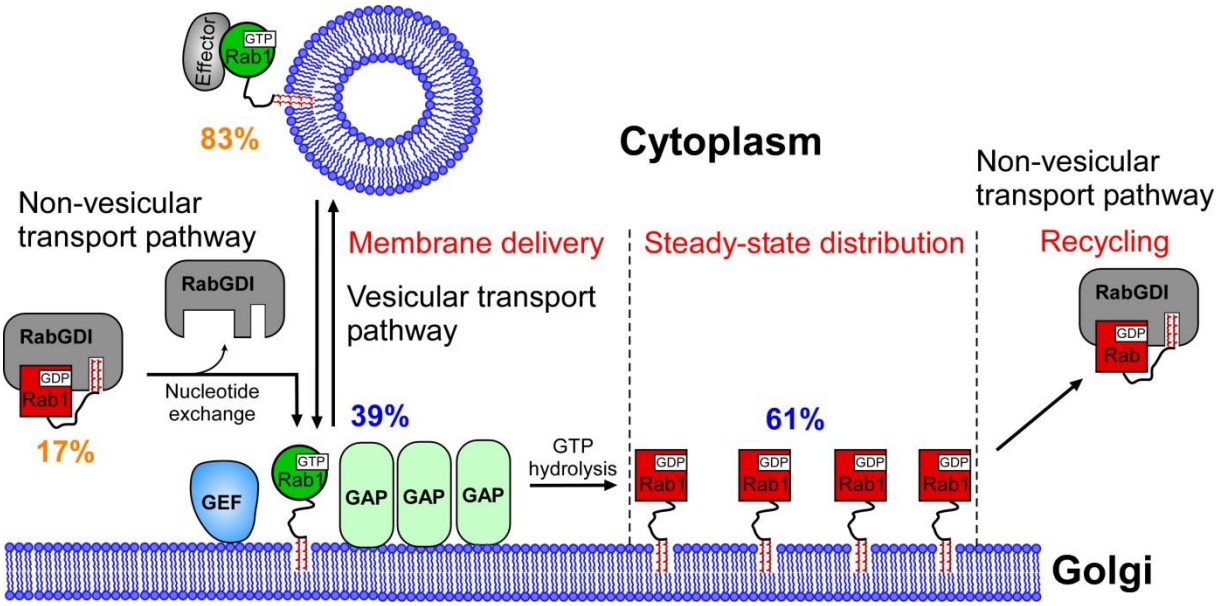

Figure S29 GTPase cycle and spatial cycle of Rab1.

Rab1 GTPase cycle coodinates spatial cycle between cytoplasm and Golgi. In the cytoplasm, 83% of Rab1 (GTP-bound) molecules are delivered to the Golgi *via* vesicular transport pathway, while 17% of Rab1 (GDP-bound) molecules are recycled between the cytosol and the Golgi membrane *via* GDI (non-vesiculart transport pathway). Rab1 molecules are largely (61%) inactivated at the Golgi and are ready for retrieval from the Golgi by GDI. 39% of Rab1 molecules are active (GTP-bound) at the Golgi, which leave the Golgi *via* vesicular transport pathway.

References

1 Schoebel, S., Oesterlin, L. K., Blankenfeldt, W., Goody, R. S. & Itzen, A. RabGDI displacement by DrrA from Legionella is a consequence of its guanine nucleotide exchange activity. *Molecular cell* **36**, 1060-1072, doi:10.1016/j.molcel.2009.11.014 (2009).

2 Grecco, H. E., Roda-Navarro, P. & Verveer, P. J. Global analysis of time correlated single photon counting FRET-FLIM data. *Optics express* **17**, 6493-6508 (2009).

3 Wu, Y. W. *et al.* Membrane targeting mechanism of Rab GTPases elucidated by semisynthetic protein probes. *Nature chemical biology* **6**, 534-540, doi:10.1038/nchembio.386 (2010).

4 Hou, X. *et al.* A structural basis for Lowe syndrome caused by mutations in the Rab-binding domain of OCRL1. *EMBO J* **30**, 1659-1670, doi:10.1038/emboj.2011.60 (2011).

5 Tang, Z. *et al.* Disruption of the EGFR E884-R958 ion pair conserved in the human kinome differentially alters signaling and inhibitor sensitivity. *Oncogene* **28**, 518-533, doi:10.1038/onc.2008.411 (2009).

6 Foster, J. M. *et al.* Clinical implications of novel activating EGFR mutations in malignant peritoneal mesothelioma. *World journal of surgical oncology* **8**, 88, doi:10.1186/1477-7819-8-88 (2010).